FRACTURE TOUGHNESS MEASUREMENTS IN A HSLA STEEL

A Thesis Submitted
in Partial Fulfilment of the Requirements
for the Degree of

MASTER OF TECHNOLOGY

by

PRABHAT TIWARI

to the

DEPARTMENT OF METALLURGICAL ENGINEERING

INDIAN INSTITUTE OF TECHNOLOGY KANPUR

APRIL, 1987

ME - 1987 - M - TIW - FRA

CERTIFICATE

This is to certify that this work entitled 'Fracture Toughness Measurements in a HSLA Steel' has been carried out under my supervision and has not been submitted elsewhere for a degree.

Dr. M. N. Shetty
Professor
Department of Metallurgical Engineering
Indian Institute of Technology
Kanpur

ACKNOWLEDGEMENTS

CONTENTS

LIST OF FIGURES

ABSTRACT

Charpy impact tests are carried out on a high strength low alloy steel over a range of temperature from room temperature to $730^{\circ}C$-a temperature slightly above the eutectiod temperature. The concept of J-integral in elasto-plastic fracture mechanics is used to determine the fracture toughness from the Charpy V Notch values. The J (converted CVN values) versus temperature plot shows three distinct regions, namely; the initial sharp rise in J values from 0 to $100^{\circ}C$, plateau region between 100 to $400^{\circ}C$ and finally the sharp rise upto $730^{\circ}C$. The plateau region is due to the dynamic strain aging. The ductile to brittle transition temperature has been found as $35^{\circ}C$ and this high value of temperature can be attributed to the presence of microconstituents, eg phospherus and sulphur in the form of manganese phosphate and Manganese Sulphide respectively. Detailed microstructural examinations is undertaken in and around the fracture zone using optical, Electron Probe micro analysis and Scanning electron microscopy to know the effect of microsonstituents on fracture toughness and transition temperature.

CHAPTER 1

INTRODUCTION

1.1 GENERAL

It has been an endeavour of engineers to predict the
failure behaviour of materials from the simple laboratory
tests on small specimens. From the structural point of view,
it is the brittle fracture which is more serious. It is charac-
terized by rapid propagation of cracks occuring at stresses
wall below the yield point and where the amount of plastic
deformation involved is very small. To measure sensitivity
to fracture suitable tests are invariably conducted on samples
bearing a notch and subjected to impact loading of some kind
at various temperatures, preferably covering the entire range
of possible service temperatures. In 1920, Griffith proposed
a theory which stated that an existing crack would propagate if
the total energy of the system would thereby be lowered. Irwin,
in 1957, proved that the   Griffith's energy approach is
equivalent to a stress – intensity approach, according to which
fracture occurs when the stresses near the crack tip reach a
critical value depending upon the material. The Griffith –
Irwin concept has then been applied in the field of fracture
mechanics. In this approach it is assumed that the behaviour
of a material near the crack tip is linear-elastic. The linear
elastic fracture mechanics (LEFM) approach then provides
quantitative expressions for the fracture stress as a function
of crack size and shape and loading conditions. But at higher

temperatures this condition becomes unrealistic because materials start behaving plastically near the crack tip. So, for the same reason extensive work has been done to extend the single parameter fracture mechanics approach into the domain of elastic-plastic behaviour of materials. Consequently two techniques of fracture toughness measurements emerged, namely, the crack opening displacement (COD) technique and the J-integral technique. Both the methods can be applied for determining fracture criterion over a range of temperatures. The J-integral technique being the most general, is particularly suited for measuring fracture toughness of materials which exhibit appreciable ductility.

The present measurements were intended to supplement our already existing set of measurements (using the J and the charpy technique) on an HSLA steel over an extended range of temperatures. In this work the J values are determined from charpy tests conducted over range of temperatures from 97^OK to 1000^OK. The method popularly known as the J-estimation procedure, is simple and accurate and compares over both the direct estimates in the earlier theories. We have examined the reasons for the dependence of the fracture toughness determined and correlated with the plastic deformation characteristics of the steel and micro structure. The microstructural investigations were carried out using optical and TEM techniques

and detailed fractography was done by SEM and microprobe
analysis of the fractured surface, to determine the factors which
have direct impact on the fracture properties of the material.

1.2 LINEAR ELASTIC FRACTURE MECHANICS

1.2.1 Energy balance approach to fracture

The study of fracture mechanics in cracked bodies by
energy balance approach was first proposed by Griffith [1]. He
proposed that a brittle material contains a very large number
of fine cracks finely dispersed and this leads to the stress
concentration of the level of theoretical fracture stress at
the crack tip, even when the applied stress is well below the
critical theoretical stress level. For the propagation of a crack
Griffith established the following criterion, 'A crack will
propagate when the decrease in elastic strain energy is at least
equal to the energy required to create the new crack surface'.
A significant step forward was the demonstration of relationship
between the fracture stress and the crack length. Griffith
equation is

$$\sigma = \left[\frac{2E\gamma s}{\pi a}\right]^{1/2} \qquad \qquad \ldots \qquad (1)$$

where σ is the stress required to propagate a crack
in the brittle material,

E is the Young's modulus,

γs is the surface energy and

a is the semi crack length.

Irwin and Orowan [2] modified the original Griffith equation so as to incorporate the limited plastic deformation prior to failure. Orowan [3] suggested the inclusion of a term r_p for the plastic deformation required to extend the crack

$$\sigma_f = [\frac{2E\ (r_s + r_p)}{\pi a}]^{1/2} \qquad (\frac{E\ r_p}{a})^{1/2} \qquad \ldots \qquad (2)$$

if the surface energy r_s term could be neglected as compared with r_p.

Orowan pointed out that if the plastic deformation was confined to thin layers adjacent to the crack walls then only the approach would be valid. He demonstrated by the modified theory that the fracture stress was directly proportional to the one over square root of crack length. However, the value of calculated from these results was 3 to 5 times greater than that expected from the X-ray analysis of the fractured surfaces. He concluded that these results would be better explained using a crack tip characterizing parameter approach.

Irwin suggested, assuming the fracture process essentially similar for different loadings and geometries, that the fracture event would occur when the strain energy release rate reached a critical value. This critical value could be regarded as a material property to be determined for a fracture test. Irwin and Kies [4] noted that the strain energy in an elastic body could be represented by the relationship

$$U = \frac{Q^2C}{2} \qquad \ldots \qquad (3)$$

where Q is the characterizing force and C the compliance
of the body, i.e. the displacement at the point of applica-
tion of Q.

From the above expression it follows that the strain
energy release rate as a function of crack extension is given by

$$\frac{\partial v}{\partial a} = \frac{1}{2} Q^2 \frac{\partial c}{\partial a} \qquad \qquad \ldots \qquad (4)$$

By measuring the compliance of a test specimen with various
crack lengths the value of $\partial c / \partial a$ as a function of crack
length could be obtained. A fracture test could be interpreted
by evaluating $\partial v/\partial a$ at fracture using the fracture load and the
value of $\partial c/\partial a$ for the appropriate crack length.

Irwin [5] proposed an alternative interpretation of
critical strain energy release rate when he suggested that this
quantity could be regarded as a force. In these terms, fracture
was described as a rate controlled process driven by this force,
which was defined as the irreversible energy loss per unit area
of newly created surface. This force denoted as G (after
Griffith) would have a critical value, G_c when a crack starts to
propagate.

In cases where there is limited amount of plastic
deformation prior to fracture, there is strict equivalence between
the strain energy release rate concept G, and the stress
intensity approach. Therefore the methods applied for deter-
mining stress intensity factors can be safely applied for

determining G. However, one has to be cautious while applying the above technique where large amount of plastic deformation takes place prior to fracture.

1.2.2 Stress intensity factor approach to fracture

Section 1.2.1 dealt with the fracture mechanics based on energy balance approach. Irwin developed the stress intensity factor approach in which the mechanical environment near the crack tip is studied.

(i) Fracture modes

There are three basic modes of fracture as shown in Figure 1. Mode I is called the 'tensile in plane' opening mode and in this mode the tensile stress is applied in the Y direction normal to the faces of the crack. Mode II is the 'in plane shearing' and the stress acts in the XZ plane. Mode III is the anti-plane shearing mode. Mode I is most important in engineering and a critical value of stress intensity determined for this mode is designated as K_{Ic}.

Irwin [6] laid the foundation for the important area of fracture mechanics. He proposed that fracture occurs at a fracture stress corresponding to a critical value of the crack-extension force, where equation 1 is rewritten as

$$\sigma_f = (\frac{EG}{\pi C})^{1/2} \qquad \cdots \qquad (5)$$

and,

$$G = \pi C \frac{\sigma^2}{E} \qquad \cdots \qquad (6)$$
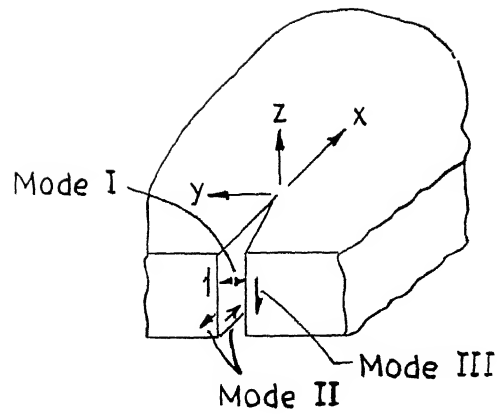
F
Fig. 1 Crack-deformation modes.
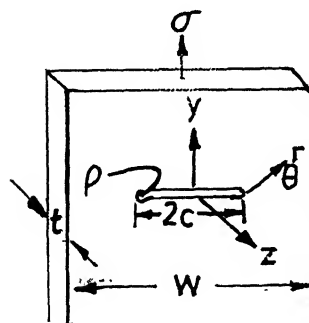
Fig. 2 Model for equations for stresses at a point
near a crack.

G may also be considered the strain energy release rate i.e. the rate of loss of energy from the elastic stress field to the inelastic process of crack extension.

ii) <u>The elastic crack tip stress field</u>

Using Westergaard's [7] complex stress functions, Irwin [8] obtained the elastic stress fields near the tip of a crack in an infinite sheet for mode I. In terms of the coordinates shown in Figure 2, the stresses are given by the following equations:

$$\sigma_x = \sigma \left(\frac{C}{2r}\right)^{1/2} \left[\cos \frac{\theta}{2} \left(1 - \sin \frac{\theta}{2} \cdot \sin \frac{3\theta}{2}\right)\right] \qquad \cdots \qquad 7(a)$$

$$\sigma_y = \sigma \left(\frac{C}{2r}\right)^{1/2} \left[\cos \frac{\theta}{2} \left(1 + \sin \frac{\theta}{2} \cdot \sin \frac{3\theta}{2}\right)\right] \qquad \cdots \qquad 7(b)$$

$$\tau_{xy} = \sigma \left(\frac{C}{2r}\right)^{1/2} \left[\sin \frac{\theta}{2} \cdot \cos \frac{\theta}{2} \cdot \cos \frac{3\theta}{2}\right] \qquad \cdots \qquad 7(c)$$

where σ=gross nominal stress = $\frac{P}{wt}$ and these equations are valid for c>r>p, and τ is the shear stress.

Irwin pointed out that the above equations indicate that the local stresses near a crack depend on the product of the nominal stress and the square root of the semi-crack length a. He called this relationship the stress-intensity factor K, where for a sharp elastic crack in an infinitely wide plate, K is given by :

$$K = \sigma \sqrt{\pi C}$$

K has the unusual dimensions of $Mn/m^{3/2}$ or $MPa \sqrt{mm}$.
Using these definitions for K, the equations for the
stress field at the end of a crack can be written

$$\sigma_x = \frac{K}{\sqrt{2\pi r}} \left[\cos \frac{\theta}{2} \left(1-\sin \frac{\theta}{2}. \sin \frac{3\theta}{2}\right)\right] \ldots \qquad 8(a)$$

$$\sigma_y = \frac{K}{\sqrt{2\pi r}} \left[\cos \frac{\theta}{2} \left(1+\sin \frac{\theta}{2}. \sin \frac{3\theta}{2}\right)\right] \ldots \qquad 8(b)$$

$$\tau_{xy} = \frac{K}{\sqrt{2\pi r}} \left[\sin \frac{\theta}{2} .\cos \frac{\theta}{2} . \cos \frac{3\theta}{2}\right] \ldots \qquad 8(c)$$

Values of K for many geometrical cracks and many types of
loading may be calculated from the theory of elasticity.
From the above discussion one can easily establish the
relationship between 'G' the crack extension force and the
stress intensity factor 'K' to be:

$$G = \frac{1+K}{8\mu} K^2 \qquad \ldots \qquad (9)$$

where μ is the shear modulus and

K is a function of Poisson's ratio ( )

viz. K = 3 - 4 for conditions of plane strain

$$= \frac{3 - \nu}{1 + \nu} \text{ for conditions of plane stress.}$$

The above relationships show that the attainment of a
critical extension force is equivalent to a critical stress
environment. Fracture in this situation can be characterized
by the attainment of a critical value of K.

Elastic analysis has shown that the stress environment around a crack tip was entirely similar to all situations to within a linear scaling factor. By means of tests on suitably shaped and loaded specimens it was possible to determine the material property K_{Ic} (or G_{Ic}) by defining it as the value of K_1 (or G_1) operative at the point of fracture. The value of K_1 at the point of fracture was found to be strongly dependent on plate thickness. Only after a certain thickness is exceeded critical value will be regarded as a material property. K_{Ic} dependent only on the testing environment. The plastic regions that are near a free surface are practically in a condition of plane stress whilst those remote from such a surface approach conditions of plane strain. When thickness is sufficient the fracture behaviour will be dominated by the region of constrained plastic deformation, a characteristic flat fracture will occur and conditions are described as 'plane strain'.

So far the basic philosophy of the stress intensity approach has been discussed without mentioning precisely how specific cases are dealt with. Obviously to interpret test results or to make design calculations, it is necessary to have explicit expressions for K_1 for specific geometries and loading conditions. Thedetermination of stress intensity factors is a specialist's task necessitating the use of a number of

analytical and numerical techniques. It would be appropriate to discuss these in a separate chapter. The important point is that it is always possible to determine K_1 to a sufficient accuracy for any given geometry or set of loading conditions.

In general stress intensity factors may be written in the form

$$K_I = \sigma \sqrt{a} \; \gamma \; \frac{a}{w} \qquad \qquad \text{....} \qquad (10)$$

where σ is a characterizing stress

a is a characterizing crack length

w is a characterizing dimension

and $Y(\frac{a}{w})$ is a calibration function which defines

K_I for the specific body under consideration.

Figure 3 shows three configurations with the corresponding values of $Y(\frac{a}{w})$. Thus for example a fracture test on a three-point bend specimen would be interpreted by substituting the appropriate value of a/W in the polynomial for $Y(\frac{a}{W})$. Figure (c) noting the load at fracture and thus determining the value of K_I at fracture. Alternatively, if it is necessary to estimate the maximum permissible depth of a surface defect in a thick component subject to uniform stress, use is made of the solution given in Figure 3(b). Here the stress intensity factor is given by

$$K_I = 1.12 \; \sigma \; \sqrt{(\pi a)}$$
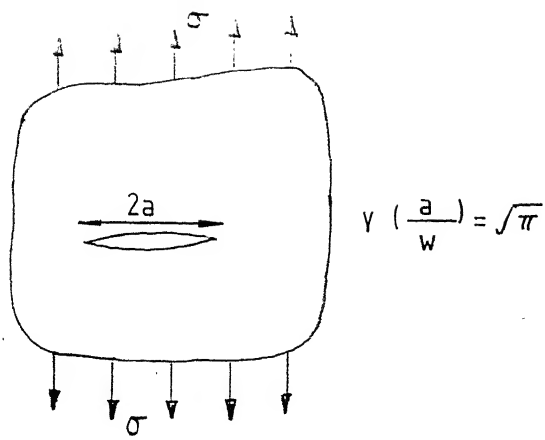
(a) Isolated crack in an infinite plate

$$Y\left(\frac{a}{w}\right) = \sqrt{\pi}$$
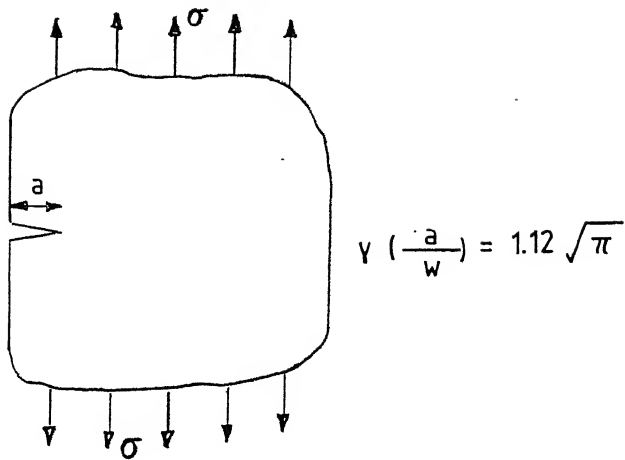
(b) Surface crack in a semi-infinite plate

$$Y\left(\frac{a}{w}\right) = 1.12\sqrt{\pi}$$

$$\sigma = \frac{6M}{tW^2} \qquad M = \frac{QS}{4}$$

t = Plate thickness

$$Y\left(\frac{a}{w}\right) = 1.93 - 3.07\left(\frac{a}{w}\right) + 14.53\left(\frac{a}{w}\right)^2 - 25.11\left(\frac{a}{w}\right)^3 + 25.8\left(\frac{a}{w}\right)^4$$
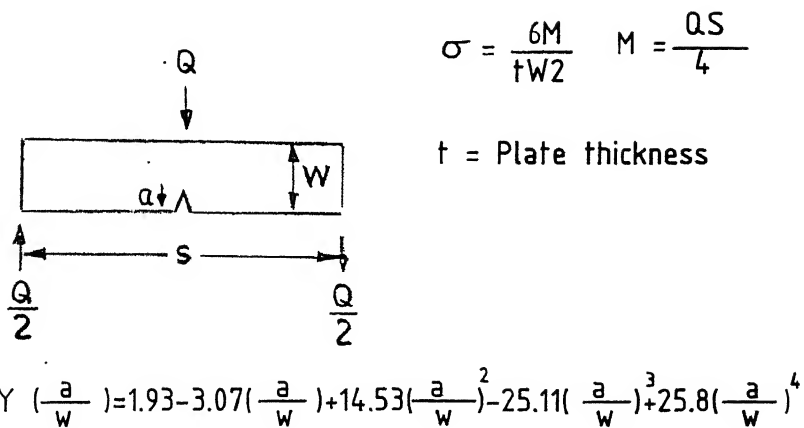
(c) Surface crack in three-point bend specimen

Fig. 3 Some crack configurations.

Consequently a knowledge of a critical value of K_I as deter-
mined by an appropriate fracture test, and the applied stress
level permits the critical value of crack depth to be deter-
mined.

To summarize, the fracture event is interpreted as
being characterized by the attainment of a critical value of
the stress intensity factor, K_{Ic}. Geometry and loading
conditions influence this environment through the parameter
K_I, which may be determined by suitable analysis. A knowledge
of K_{Ic} obtained from a suitable test, thus provides a means
of predicting the fracture behaviour in real structures.
The sensitivity of structures to other phenomena such as
fatigue crack growth and stress corrosion cracking can like-
wise be predicted on the basis of suitably performed tests
interpreted in terms of the stress intensity approach.

1.3 YIELDING FRACTURE MECHANICS

Yielding fracture mechanics deals with the fracture
prediction in ductile materials having a defect. In this
approach also fracture measured in the laboratory is described
as the material property, toughness. In yielding fracture
mechanics also efforts have been made to characterize the
elastic-plastic stress and stress fields near the crack tip
by a single parameter. If this single parameter is evaluated

then the critical value of it would cause fracture for a given set of constant conditions i.e. material composition, temperature, strain rate etc.

1.3.1 The role of extent of plasticity

The notion of plastic constraint and associated terms such as small scale or contained yield and constrained or unconstrained yielding into proper perspective, the different ways in which a cracked component may fail when loaded beyond the range to which LEFM is applicable will now be surveyed briefly. A centre-cracked panel loaded in tension is taken as a simple example.

A stress very near to the crack tip (not specifically defined here but taken as representative of the local stress conditions) is denoted by the L^{σ} the uniaxial yield stress by σ_y, net section stress by $_n$ and the uniform stress remote from the crack by σ. It is useful to distinguish four regimes, which can loosely be described as follows.

(a) $L^{\sigma} > \sigma_y > \sigma_n > \sigma$: Yielding limited to a zone in the immediate vicinity of the crack, to a very small extent. This is the LEFM problem. If failure occurs it is usually by unstable, rapid propagation of the crack.

(b) $L^{\sigma} > \sigma_y > _n > \sigma$: Yielding is extensive but does not spread to a lateral boundary of the structure and thus contained. This is a regime that can be called elastic-plastic and

to which yielding fracture mechanics can be applied. Failure usually occurs by unstable rapid propagation of the crack.

(c) $L^\sigma > \sigma_n > \sigma_y > \sigma$: Yielding is very extensive and spreads to the lateral boundary ahead of the crack, and thus uncontained. This is the regime that can be called gross yield, to which yielding fracture mechanics must be applied. For configurations with little lateral constraints and low hardening, though materials may fail by plastic collapse of the net section, whilst for less tough materials a crack may spread by stable or unstable growth.

(d) $L^\sigma > \sigma_n > \sigma > \sigma_y$: Since the applied stress is greater than the yield stress, extensive plasticity occurs along the components as well as the cross section implying work hardening of the net section. This is the regime that can be called general yield. Crack propagation in this case may still be the failure mode.

These four conditions are shown schematically in Figure 4. It must be clear that the stress levels used to describe the four states merge from one condition to the other and are affected by configuration, induced biaxial and triaxial stresses and work hardening. Clearly, the regimes starting in (b) and extending through (c) and for some materials
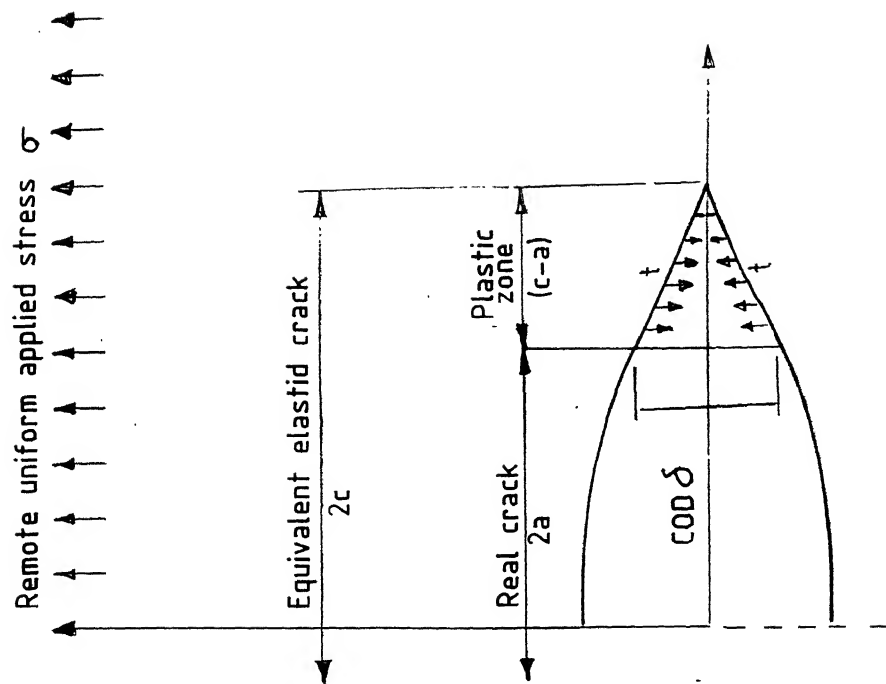
Fig. 5 The Dugdale model for crack tip plasticity.
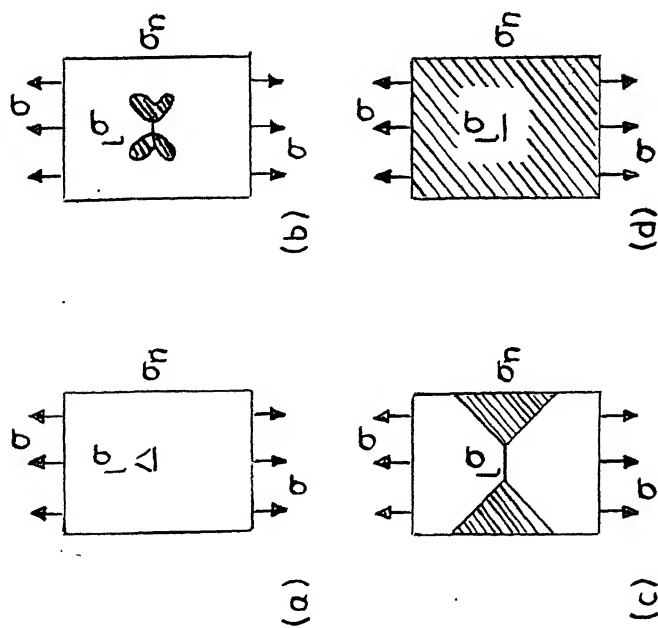
Fig. 4 Schematic representation of increasing degrees of yielding.

into (d) are those that constitute the realm of yielding fracture mechanics of interest here.

1.3.2 Concept of crack opening displacement (COD)

Wells [9], Cottrell [10] and Bav.enblatt [11] proposed independently that in cases where significant plasticity is involved, the fracture process would be dependent on the intense deformations near the crack tip and it turns and that the separation of the crack faces, or crack opening displacement is the measure of the intense deformation.

Crack propagation will start at same critical value of this crack opening displacement. Therefore, it is required to predict the displacements near the crack tip, analytically.

The model, proposed by Dugdals [12] and Barenblatt [11] considers an infinite plate with a central crack, length 2a, subjected to a remotely applied uniform stress. The plasticity at the tip of the crack is represented by a notional increase in the crack length to some value, 2c with the faces of the 'crack' over the distances (c-a) from both ends partly restricted from opening by a restraining stress, 't' acting directly on the crack faces. Later, Wells [13] noticed that in practice the tip of a slot subjected to plastic deformation opened with a near square ended contour, giving a definite tip opening - the crack opening displacement - (COD) as in Figure 5. He proposed that the COD, δ, was a measure of crack tip deformation and that fracture might occur when a

critical value of this parameter, δ_c, was reached. This proposal was pursued experimentally and theoretically by many scientists who have showed that it was broadly consistent with fracture results from large tension and bending tests.

In early applications of this model, t was equated to the uniaxial yield stress, and relationships obtained for the length, 2c, to which the notional plastic zone extended in terms of the real length, 2a, and the applied stress σ

$$\frac{a}{c} = \cos \frac{\sigma\pi}{2\sigma_y} \qquad \cdots \qquad (11)$$

The COD, δ, at the tip of the real crack was then evaluated as

$$\delta = \frac{8\sigma_y a}{\pi E} \log \sec \frac{\pi\sigma}{2\sigma_y} \qquad \cdots \qquad (12)$$

By expanding the second term it was found that

$$\delta = \frac{\pi\sigma^2 a}{E\sigma_y} \left[1 + \frac{\pi^2}{2}\left(\frac{\sigma}{\sigma_y}\right)^2 + \ldots\ldots \right] \qquad \cdots \qquad (13)$$

However renumbering the defintion of strain-energy release rate in LEFM, for the infinite plate with centre crack 2a

$$G = \frac{K^2}{E} = \frac{\pi\sigma^2 a}{E} \qquad \cdots \qquad (14)$$

It is at once seen that the first term in equation 13 corresponds to

$$G = \sigma_y \qquad \cdots \qquad (15)$$

If the plastic zone correction factor for plane stress is used then the modified LEFM expression is

$$G = \frac{\pi\sigma^2 a}{E}[\ 1 + \frac{1}{2}\ (\ \frac{\sigma}{\sigma_y}\ )^2] \qquad \ldots \qquad (16)$$

which together with equation 15 differs from the equation 13 by a fairly small amount in the coefficient of the second. term. The relationship $G = t\delta$ is consistent with the work done to close an element of crack, from the reasoning of mechanics on either the macro or dislocation level, so that this model used with the restraining stress $t = \sigma_y$ appears to be a logical extension to LEFM for plane stress.

Turning to the weaknesses in the model, the most obvious of these is the representation of plastic yielding by an elastic material with only a line of plasticity ahead of the crack. This is not unreasonable for plane stress but unrepresentative for plane strain. For reasons that are not wholly apparent, the usage of the Dugdale model has retained the plane stress assumption of $t = \sigma_y$. It has in fact suggested that this inconsistency might be avoided through the use of a constrained yield stress

$$t = m.\ \sigma_y \qquad \ldots \qquad (17)$$

where m might be $\sqrt{3}$ (from plastic zone correction) or even as high as 3 for yielding material analysed for contained yielding.

Still by using these modified expressions for finding the fracture criteria there exists some discrepancies between theory and experiment. Thus the above model ignores the effect of a finite plate and of a work hardening material.

1.3.3 Concept of the J - integral

The J - integral method proposed by Rice [14] to correlate the elastic-plastic fracture behaviour is the most widely applied. By this method the stress and strain at the crack tip are determined analytically. It was first proposed as a fracture parameter, labelled J_{Ic}, with supporting experimental method proposed was fairly cumbersome. Easier experimental methods for determining J_{Ic} have been developed. A considerable amount of new work has been conducted both in supporting the use of J_{Ic} as an elastic-plastic fracture criterion and in developing the testing techniques for determining J_{Ic}.

(a) J-theory in general

The J-integral as proposed by Rice [14] is a two dimensional energy line integral (ref. Figure 6):

$$J = \int \left(W \, dy - x \frac{\partial u}{\partial x} \, ds \right)$$

where W is the strain energy density

$$W = \int_{0}^{\epsilon_{mn}} \sigma_{ij} \, \epsilon_{ij} \qquad \qquad \dots \qquad (19)$$

is the traction vector defined by the normal n along the path of integration, $T_i = \sigma_{ij} n_j$, u is the displacement vector, and S is a length along. The J-integral is path independent and is applicable to elastic material or elastic-plastic material when treated by a deformation theory of plasticity.

The J-integral characterizes the crack tip field the basis of which is provided by the works of Hutchinson [15] and Rice and Rosengren [16]. They have extended fracture mechanics concepts to cases of large scale yielding which also assumes the crack tip singularity. They indicate that the product of plastic stress and strain approaches a $\frac{1}{r}$ singularity; r being a near tip crack field length parameter. The crack tip singularity is uniquely dependent on the material constitutive relations. For a deformation theory of plasticity McClintock [17] has demonstrated, through the crack tip plastic stress and strain equations expressed from the Hutchinson, Rice, Rosengren (HRR) singularity, the existence of singularity in r whose strength is the J-integral.

The J-integral has another important advantage as a fracture criterion. Broberg [18] considered growth criteria for a nonlinear elastic body containing a crack. For such a body, stress and strain singularities occur at the crack tip. This region ahead of the crack tip is termed as the end region outside which the material may be regarded as a continuum. As the load is increased, the end region
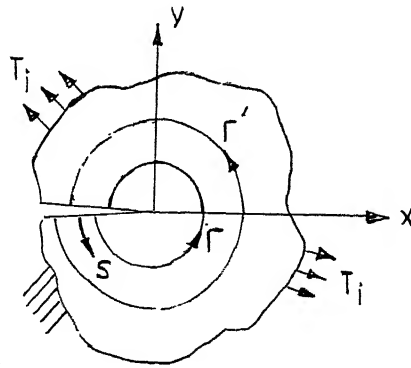
Fig. 6 Arbitrary contour over which J integral is evaluated

1. ══════ Fatigue crack

2. ══════⊃ First loading

Fracture toughness
measurement point

3. ──────) Crack blunting

4. ──────⟩ First crack advance

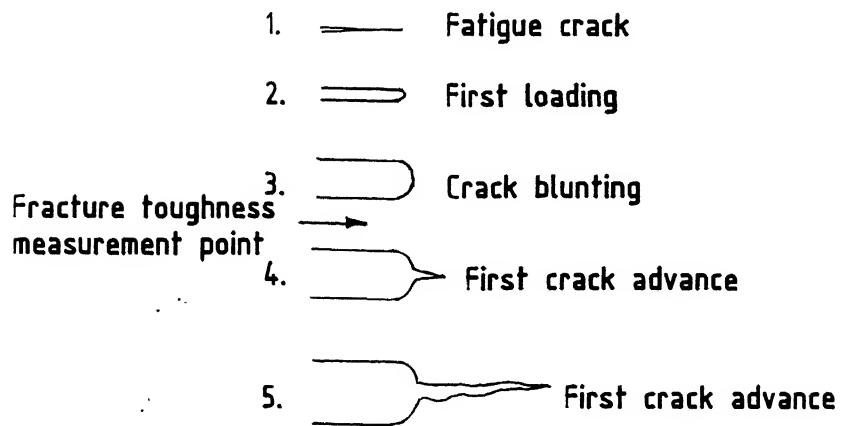5. ──────⟩─── First crack advance

Fig. 7 Crack-tip schematic of the fracture process

eventually reaches a critical state at which the crack starts moving. One prominent feature of the end region at critical state is that the state is neither dependent on the distribution of loads nor on the crack length. It simply and solely depends on the material itself. The end region or plastic zone can be specified by J_c, as it reaches the critical state.

From the foregoing discussion, it is evident that J-integral displays three prominent features attractive to its use as a fracture criterion namely,

(i) J-integral as a field parameter indicates the stress and strain distribution in a cracked body.

(ii) It describes the crack tip region by specifying the strength of the singularity.

(iii) Critical value of J-integral, J_c is a material property which can be used as a fracture criterion.

The J-integral can be conveniently evaluated experimentally through its energy rate interpretation as follows. It may be noted that in equation (5) the two terms in the integral namely W and $T_i \frac{\partial u_i}{\partial x_i}$, have the dimensions of energy. Thus, J is an energy related quantity. In fact, Rice [14] has shown that the J-integral is equal to the change in potential energy for a virtual crack extension

$$J = -\frac{\partial u}{da}$$ ... (20)

Where u is the potential energy per unit thickness

a is the crack length.

Equation (20) expresses an energy process where J is identical to G, the crack driving Force. For the case of plastic behaviour where deformation is not reversible, J loses its significance as a crack driving force. It can be considered as an energy comparison between two similar bodies identically loaded which have incrementally differing crack sizes. The line integral definition of J in Equation (18) is most useful for an analytical determination of J where numerical methods are employed. The energy rate interpretation is used for experimentally determining J. Equation (19) represents an exact method for experimentally measuring J; however, for most testing purposes, an approximation to Equation (3) is used.

(b) <u>Limitations of J_{Ic} approach</u>

(i) Since the Rice energy line integral is expressed only in two dimensions, the J approach is therefore, limited to problems of plane strain or generalised plane stress.

(ii) Another limitation is that since J is shown to be path independent for deformation plasticity theory, the use of J as a fracture criterion should be compatible with the assumptions of deformation plasticity. This would restrict its use to monotonic loading and zero crack

extension since any unloading cannot be treated by this theory of plasticity. Any crack extension necessarily implies unloading near the crack tip. In general, structures failing in plane stress exhibit some subcritical crack growth. Hence, the J integral failure criterion may be limited to the case of plane strain which is implied by the subscript I in J_{Ic}.

(iii) Also, since J is taken as the single parameter which characterizes the strength of the crack tip singular field equations, the size of the test specimen must be sufficient so that the crack-tip field equations are undisturbed by the specimen boundaries.

(c) <u>J as a fracture criterion</u>

The fracture process starts with a sharp crack when the specimen or structure containing the crack is unloaded. For a test specimen the crack is introduced by fatiguing at a low k level before the fracture test is conducted. As the crack undergoes loading the crack tip becomes blunted. This blunting increases with an increase in loading until a load is reached where a crack advance occurs ahead of the original blunted crack (ref. Figure 7). At the point where the first crack advance occurs the fracture toughness measurement point is defined. In terms of J this point is labelled J_{Ic}.

This model may not strictly characterize the actual physical process. Cracking may begin ahead of the original blunted crack as voids are opened and joined. However, this model gives a general description of the fracture process which can then be related to a fracture parameter such as J. A physical application of the model is conceived more easily when cracking occurs in a ductile tearing mode.

1.4 METHODS FOR FRACTURE TOUGHNESS MEASUREMENT

Standard test method for the determination of K_{Ic} has been approved by ASTM. (Ref. Standard Test Method for Plane Strain Fracture Toughness of Metallic Materials-ASTM Designation E399-74). The ASTM procedures have been devised so as to permit measurement of K_{Ic} and displacement (COD) under identical conditions with the some laboratory equipment and in the same test.

The unified testing procedure is :

1. A machined notched test piece is used in which a tensile stress is developed at the notch tip either by tension or by bending.

2. The test piece is subjected to fatigue loading to start a sharp crack and develop it to the desired length.

3. The test piece is then loaded in tension or bending and a record is taken of the load against the opening

displacement of the two sides of the notch. The test
is continued until fracture occurs.

4. The fracture toughness parameters are calculated from
the load,   displacement and initial crack length.

1.4.1 K_{Ic} testing

(a) Types of test piece

Two main types of test pieces are recommended.

(i) Bend test pieces: These are the simplest and cheapest
to machine. Limitations are imposed upon the test piece
dimensions and the shape and depth of the notch. The pieces
most commonly used have $B = \frac{1}{2}$ W, a[0.45W, to 0.5W, where B
is the thickness, W is the width and a the crack length
of the specimen.

(ii) Compact tension test pieces: The specimen tension test
pieces use less material, but the cost of machining the
Clevis pinholes accurately is considerable. The recommended
dimensions are $B = \frac{1}{2}$ W, a=0.45 to 0.55W and 2F=0.275 W.
(Refer to Figure 8).

(b) Testing Fixtures

To reduce friction to a minimum, bend tests are made
on freely rotating rollers with or without fixed centres.
The diameter of the rolls and centre of loading point should
be between $\frac{1}{3}$ W and W.

(c) <u>Test piece dimensions</u>

The plane strain fracture toughness of a material is a measure of its resistance to unstable fracture under conditions where plastic deformation is limited to a region of the crack tip which is small in comparison to the test piece size, but the manner and the degree in which plasticity is to be limited is confirmed recently.

This is achieved by restricting the nominal stress at the cracks tip to below the yield stress. The nominal stress is the stress that would exist at the crack tip if there were no stress intensification there.

In a compact tension test piece:

$$\sigma_{nom} = \frac{2Q(2W + a)}{B(W - a)^2} \qquad \ldots \qquad (21)$$

and in a bend test piece:

$$\sigma_{nom} = \frac{3QL}{B(W - a)^2} \qquad \ldots \qquad (22)$$

where Q is the applied load.

ASTM special committee has accepted the recommendation that the nominal stress should not exceed O percent of the 0.2 percent proof stress.

Another requirement is that is to limit plastic deformation by maintenance of plane strain conditions at the crack tip. According to the standardized procedure to ensure plane

strain ASTM 24, consistent K_{Ic} values could be obtained
if

$$a, B > 2.5 \left(\frac{K_{Ic}}{\sigma_y} \right)^2 \qquad \ldots \qquad (23)$$

where a is the crack length

B is the thickness of the test piece.

Moreover, a/W values greater than 0.55 were considered
undesirable because at high a/W values small errors in crack
length can give rise to large errors in K_{Ic}:

(d) Fatigue pre-cracking

   Basic requirements for the fatigue pre-cracking:

   (a) The ratio of minimum to maximum force shall be in the
       range of 0 to 0.1.

   (b) K_f shall not exceed 0.7 $(\sigma_{y_1}/\sigma_{y_2})$ K_Q where σ_{y_1} and
       σ_{y_2} are the proof stresses temperatures of fatigue
       cracking and at the test temperature respectively.

   (c) The crack length shall not be less than 1.25 mm and
       the a/W ratio shall be in the range 0.45 to 0.55.

   After testing the crack is measured and the effective
crack length is measured from the average of three measurements
at 25, 50 and 75 percent B.

(e) Instrumentation

   A fracture toughness test is conducted in much the
same way as a tensile test, the extensometer to measure
strain being replaced by a gauge located across the notch of
the test piece to measure the crack opening displacement.

(f) The offset procedure

K_{Ic} values were originally calculated from the pop-in load illustrated in Figure 9. Type IV since many materials do not exhibit pop in a procedure is established to determine K_{Ic} values from force-displacement records showing deviations from linearity but no sudden discontinuity i.e. type I, Figure 9. The secand intercept procedure is adopted for this purpose.

The procedure is as follows. Referring to Figure 9 draw the secant line OQ_5 through the origin with slope 5% less than the tangent OA to the initial part of the record. Draw a horizontal line representing a constant force of 0.8; Q_Q; q_i is the distance along this line between OA and the curve record. If this deviation from linearity at the force of $0.8Q_Q$ is more than 1/4 of the corresponding deviation, q_1 at the force of Q_5 excessive non-linearity is present and so the curve is rejected.

So, for this situation the test piece of greater thickness should be selected and the experiment is to be repeated for K_{Ic}.

(g) Calculation of K_{Ic}

The stress intensity factor at the tip of a crack of length 2a, for the three point bending is given by
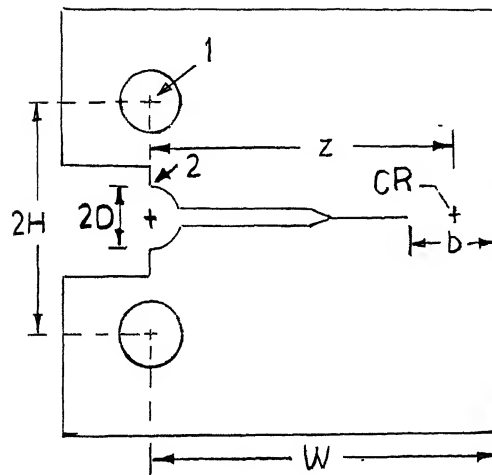
$$K = \frac{QY}{BW^{1/2}} \qquad \cdots \qquad (24)$$

Fig. 8 Schematic of compact specimen 1, load point,2,
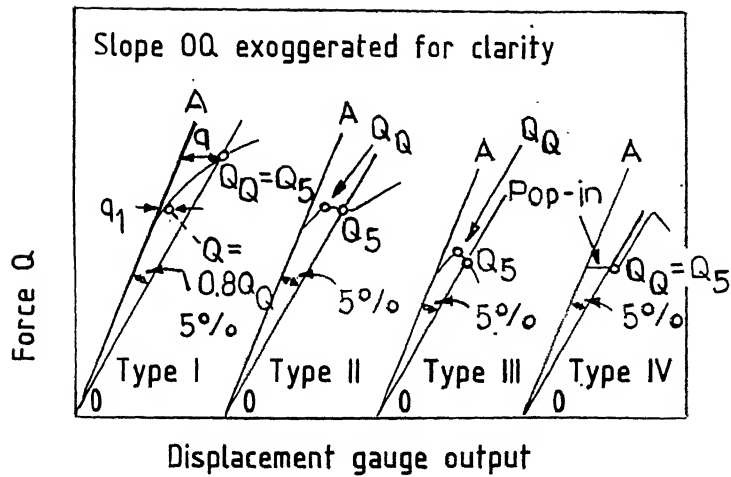displacement point, CR, centre of rotation.

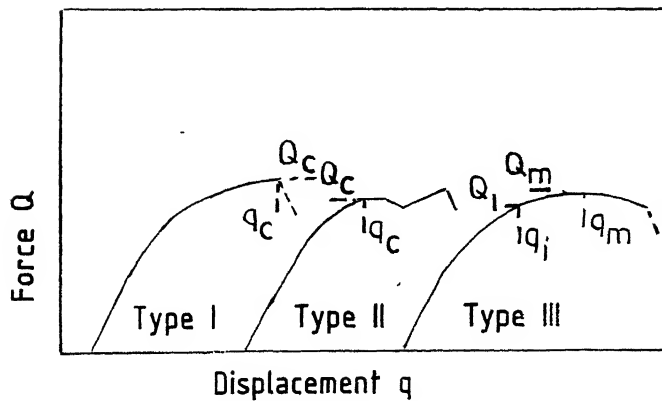Fig. 9 Schematic force /displacement records showing quantities involved in analysis.

Fig. 10 Force /displacement records for calculation of COD

Where Y is the compliance function derived from the relation-
ship between test piece compliance and dimensionless crack
length a/W i.e.

$$Y = f(\frac{a}{W})$$

$$= 1.93(\frac{a}{W})^{1/2} - 3.07(\frac{a}{W})^{3/2} + 14.53(\frac{a}{W})^{5/2} - 25.11(\frac{a}{W})^{7/2}$$

$$+ 25.80(\frac{a}{W})^{9/2} \qquad \ldots \qquad (25)$$

These values are given in tabular form for values of a/W
between 0.45 and 0.55 in increments of 0.001 (a/W).

1.4.2 COD testing

Both COD and K_{Ic} tests are performed using a unified
testing procedure and therefore employ similar test pieces,
fatigue pre-cracking procedures, testing procedures and analysis.

The crack opening displacement is a measure of the
resistance of materials to fracture initiation under conditions
where gross plastic deformation occurs and linear elastic
fracture mechanics becomes invalid. The main objective of
the COD test is to determine the critical crack opening dis-
placement at the tip of a sharp crack at the onset of crack
extension. This is done by measuring the displacement at the
mouth of the notch using a gauge identical to that used in
K_{Ic} tests and by performing a suitable calculation.

Testing

The test record consists of a plot of force Q versus crack opening displacement at the notch mouth measured by a displacement transducer. A typical record is shown in Figure 10 where the critical displacement q_c at instability is the total value corresponding to the maximum applied force Q_c, Figure 10. In the case of type II, if the falling load portion can be shown to be associated with crack growth, by electrical potential method or by an audible sound, then q_c is measured at the discontinuity shown. The third type of record where there is no sudden discontinuity is associated with slow crack growth which commences during the rising portion of the test record. An electrical potential method must be used to detect at the initiation of stable crack growth δ_i.

In those cases where crack growth cannot be measured the crack opening displacement δ at the displacement q_m corresponding to the first attainment if a maximum load can be used.

Several methods have been proposed for converting q_c values to and used in practice.

1.4.3 J-determination techniques

i) Compliance J

The J-integral can be conveniently evaluated through the energy release rate interpretation of J as derived by

Rice [14]. As explained earlier, J may be written for non-linear elastic material with no crack advance as:

$$J = -\frac{1}{B} \frac{\partial u}{\partial a}\Big|_u = \frac{1}{B} \frac{\partial C}{\partial a}\Big|_F \qquad \cdots \qquad (26)$$

where F is the applied load

   u is the load point displacement and

   c is the complementary energy $\int q \, dF$;

In the case of plasticity, where deformation is irreversible and J cannot be interpreted as the energy available to drive the crack, the contour integral J is numerically equal to

$$-\frac{1}{B} \left[\left(\frac{\partial u_{el}}{\partial a}\right)\Big|_u + \left(\frac{\partial u_{pl}}{\partial a}\right) \right] \qquad \cdots \qquad (27)$$

This represents the energy difference for monotonically loaded cracks cut initially to different lengths.

Using equation (26) J may be experimentally evaluated as follows. For convenience, displacements are prescribed as boundary conditions. Hence, the second term of the J integral in equation (18) drops out i.e., the potential energy becomes equal to the integral of the strain energy which is simply equal to the work done on the body.

The J-integral can be evaluated considering the load deflection diagrams of similar bodies with neighbouring crack sizes. When two similar bodies with crack lengths a and a+ a are loaded, the load deflection curves are represented

by OA and OB. If in the first body, the crack extends from a to a = a under prescribed load F_o, the total work done on the body is represented by the area OABCO (Figure 11(b)). Because of reversibility, the unloading curve from the point B is the same as the loading curve of the body starting with a crack length, a +Δa. The strain energy of the body with a crack length a +Δa, under the load F_o is the area OBCO. The shaded area OABO (-ΔU) is the energy available for crack extension. Similarly when the crack extends from a to a + a under prescribed displacements, the energy available for crack extension is the shaded area OABO (Figure 11(b)).

At any given displacement, the area under the load versus load point displacement record may be found for bodies with different crack lengths. The slope of the plot U versus 'a' at a given displacement is $\frac{\partial U}{\partial a}\big|_V$ and hence J be determined. This process is shown schematically in Figure 12. The final plot is J versus the applied displacement. In general, this curve depends on the crack length a. If the applied displacement is found for the initiation of crack growth, the critical J value, J_{Ic} may be found.

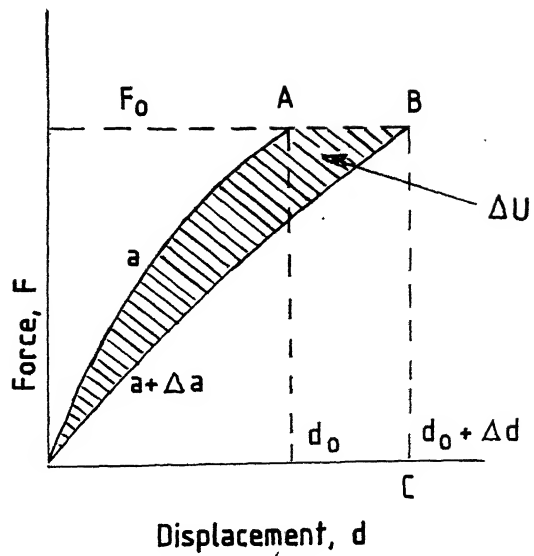(ii) $\underline{J_{Ic} \text{ testing using Rice et al estimation procedures}}$

A compliance determination of J, while possessing the advantage of generality, is tedious and expensive in both time and material and therefore is no longer used to determine experimentally. A significant advance in fracture tough-
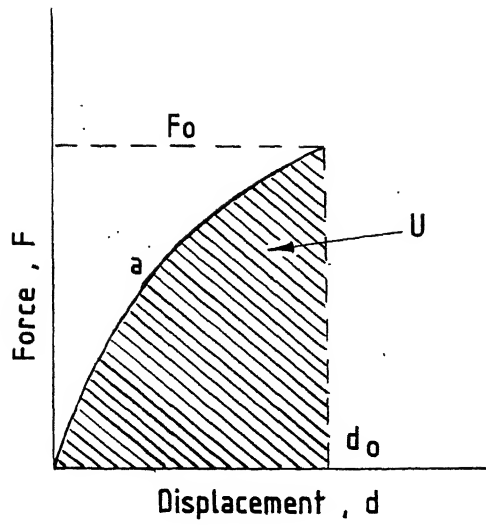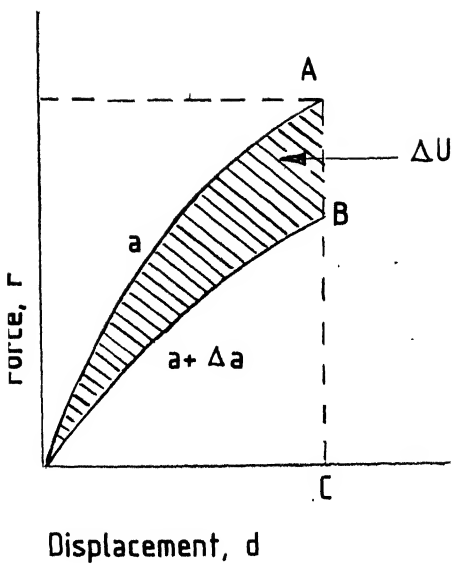
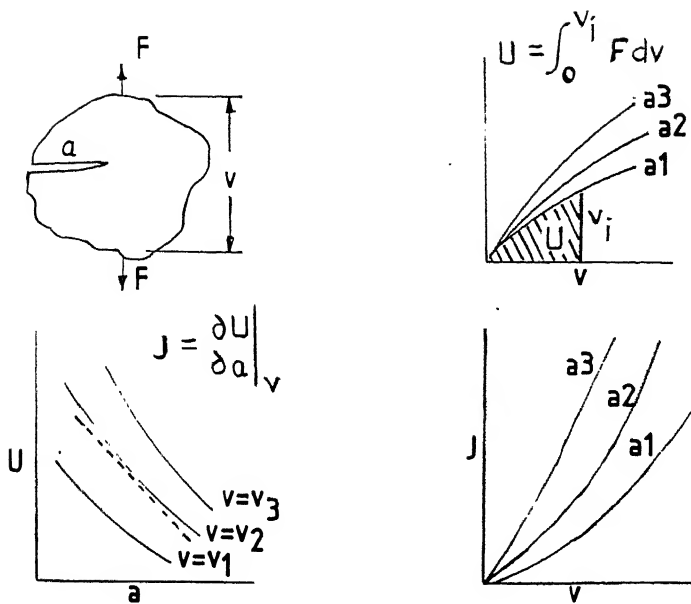Fig. 11 Schematic load-displacement curves with prescribed load/displacement.

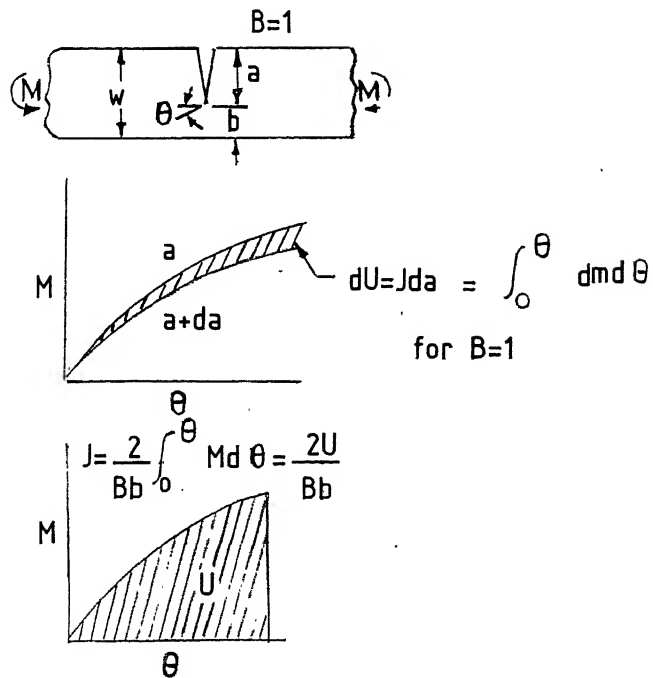Fig. 12 Schematic of steps in a compliance J determination

Fig. 13 Schematic showing Rice-Paris-Markle J formula for bend type specimen.

ness testing was provided by the development of the Rice-paris-Merkle J formula for deeply cracked bars subjected to bending [19]. This same method has been made use of in our present study of the determination of J for the HSL steel.

(a) The Rice-paris Merkle J

The derivation of this formula is based on the fact that the angle of bend θ, for deeply cracked bars, is only a function of the applied moment M and the square of the remaining ligament, b (Ref. Figure 13)

$$\theta = f\left(\frac{M}{b^2}\right) \qquad \cdots \qquad (28)$$

Using the potential energy definition of J given by equation (26) and the fact that da is equal to -db, J can be written as

$$J = \frac{1}{b} \int_0^\theta \left.\frac{\partial\theta}{\partial a}\right|_N \, dM$$

$$= -\frac{1}{B} \int_0^\theta \left.\frac{\partial\theta}{\partial b}\right|_M \, dM \qquad \cdots \qquad (29)$$

This is schematically illustrated in Figure 13. From equation (14)

$$-\left.\frac{\partial\theta}{\partial b}\right|_M = -f'\left(\frac{M}{b^2}\right) \left.\frac{\partial(M/b^2)}{\partial b}\right|_M = \frac{2M}{b^3} f'\left(\frac{M}{b^2}\right) \cdots (30)$$

Similarly

$$\left.\frac{\partial\theta}{\partial M}\right|_b = \frac{f'(M/b^2)}{b^2} \qquad \cdots \qquad (31)$$

and thus

$$-\left.\frac{\partial\theta}{\partial b}\right|_M = \frac{2M}{b} \left(\frac{\partial\theta}{\partial M}\right)\Big|_b \qquad \cdots \qquad (32)$$

Substituting equation (32) in equation (29)

$$J = \frac{2}{Bb} \int_0^M M . \frac{\partial \Theta}{\partial M} \Big|_b \, dM$$

$$= \frac{2}{Bb} \int_0^\Theta M . \, d\Theta \qquad \qquad \dots \qquad (33)$$

Yields the result that J is simply related to the work done on the specimen. Again the above derivation holds true for deeply cracked bars in bending such that Θ is only a function of M/b^2. The concept of relating J to the work done on the specimen is one that is used almost exclusively in present test methods.

(b) <u>Testing procedure</u>

From the discussion above, it is learnt that this method is based on the approximate formulation for calculating J given by Rice et al

$$J = \frac{2A}{Bb} \qquad \qquad \dots \qquad (34)$$

where B = specimen thickness

      b = remaining uncracked ligament of the specimen,

and   A = area under the load versus load point displacement
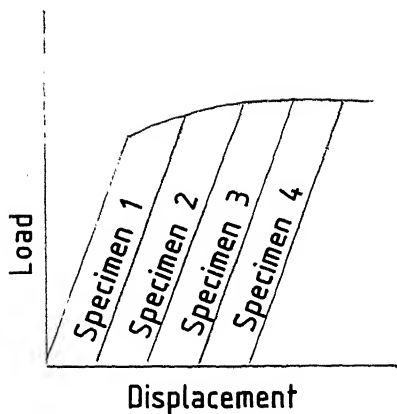
          curve.

This formulation applies to a specimen with a deep crack subjected to a bend type of loading. The types of specimens most suited to this formulation are the compact toughness specimen (CT) and bend bars with three point loading.

The method proposed for determining the J_{Ic} measurement point is shown schematically in Figure 14. Several identical specimens are loaded to differing values of displacement and then unloaded (Figure 14 (a)). These specimens will hopefully all exhibit different amounts of crack growth. After unloading, the crack advance is marked and the specimens broken open so that the crack advance, a, can be measured (Figure 14(b)). Different methods can be used to mark the crack advance. For steels the easiest method is heat tinting. The specimens are heated about $600^{o}F$ for about 10 min. The specimens subsequently are broken open at liquid nitrogen temperature. The value of J at the point where the specimen is unloaded is determined from equation (20) for each specimen (Figure 14(c)). This value of J is plotted as a function of crack advance (Figure 14(d)).

The curve in Figure 14(d) is the crack growth resistance curve from which J_{Ic} is determined. The present method for determining J_{Ic} uses the blunting line define as

$$J = 2 \, \sigma_{flow} \cdot a \qquad \qquad \ldots \qquad (35)$$

The point where additional crack advance occurs from the blunted crack, that is the J_{Ic} measurement point, is marked by a change of slope in the curve of J versus crack extension. The points on the plot which lie to the right of the blunting line are generally filled with a straight line and J_{Ic} is taken at the intersection of this fitted line and the blunting line.

(a) Load identical specimens to different displacements
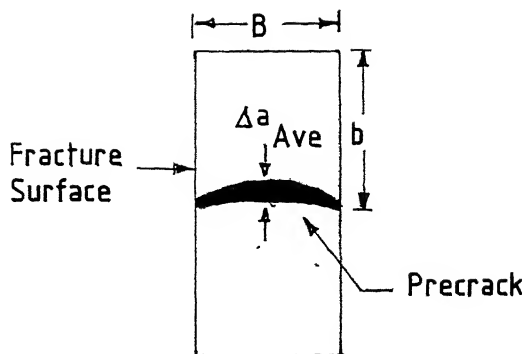
(b) Heat tint and measure average crack extension

$$J = \frac{2 \text{ Area}}{Bb}$$
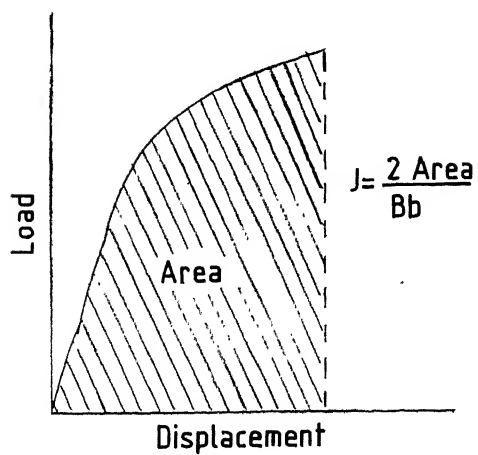
(c) Calculate J for each specimen.

Blunting line $J = (2\sigma_{flow})(\Delta a)$
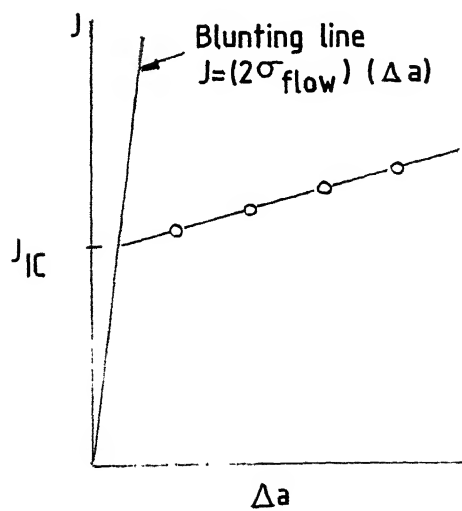
(d) Plot J vs Δa find J_{IC}

Fig. 14 Procedure for experimental J_{IC} measurement: multiple specimen R-curve.

The method for determining J_{Ic} as described by Figure 4 is presently used as a standard method. Certainly some aspects of this method can be improved. Most notably perhaps is the method of analysing the date points in Figure 14 (d) to obtain J_{Ic}. This analysis is somewhat objective and can possibly lead to ambiguous values of J_{Ic}. The use of the approximation formula from equation (34) has been compared experimentally with the original energy rate definition of J, equation (3) and found to compare favourably for a/W > 0.6.

Fatigue pre-cracking of specimens

Specimens should be precracked in fatigue with a maximum permissible load not exceeding one fourth P_L, which can be calculated from the following

$$P_L = (\frac{4}{3}) \frac{Bb^2 \sigma_{flow}}{S} \quad \text{for the bind specimen} \quad (36)$$

where b is uncracked ligament, B is the specimen thickness, S is the specimen bend span and σ_{flow} is the flow stress. Fatigue cracking should be conducted at a sufficiently low load so that the crack tip is not overloaded. The J_{Ic} test is expected to go into the plastic regime which means that specimen will most probably reach limit load.

(c) Limitations of this J_{Ic} testing

One important limitation on the test method is specimen size needed to determine a J_{Ic} value. This size limitation is generally expressed by

where B, a, are the specimen thickness, crack length respectively. α is a non-dimensional constant taken to be somewhere in the order of 25 to 50. These values in fact differ from one material to another depending on such things as the degree to which the material starain hardens.

Another important limitation on the use of the present J_{Ic} test methodology lies in the specimen type. The approximation formula for J given by equation (34) has been formulated only for bend type specimens. Although approximations exist for other types of specimens, care should be exercised whenever a specimen other than a CT or bend bar is used.

1.4.4 New test methods

With the use of equation (34) J can be determined for a single specimen at any given value of displacement. To determine the whole curve of J versus Δ a hence J_{Ic} from a single specimen all that is needed is a continuous monitor of crack advance during the generation of the load-displacement curve. Several methods have been demonstrated which can accomplish this successfully. They are namely elastic compliance method, electrical potential method and ultrasonic method.

CHAPTER 2

EXPERIMENTAL PROCEDURE

The high strength low alloy steel in the present investigation had the following composition (in weight %);

C	Mn	S	P	Mn	Nb	V	Ni	Cr	Cu
.185	.16	.019	.014	.96	.062	.006	.013	.015	.011

The regular mechanical properties of the steel were determined using standard tensile test specimens recommended. by ASTM and tabulated.A micrograph of the steel under study in as received condition is shown in Fig. (15).

Mechanical properties

0.2% yield strength	- 430 Mn/m^2
Ultimate strength	- 525 Mn/m^2
Elongation	- 27%
Room temp. charpy energy	- 35.26

Charpy impact test was carried out over a range of temperature in order to correlate fracture toughness with other mechanical properties.

2.1 NOTCHED BAR IMPACT TEST

2.1.1 Specimen design and preparation

Samples were cut from the block of HSLA steel obtained from Steel Authority of India Limited, Ranchi, manufactured by IISCo. Samples were prepared keeping in mind that the
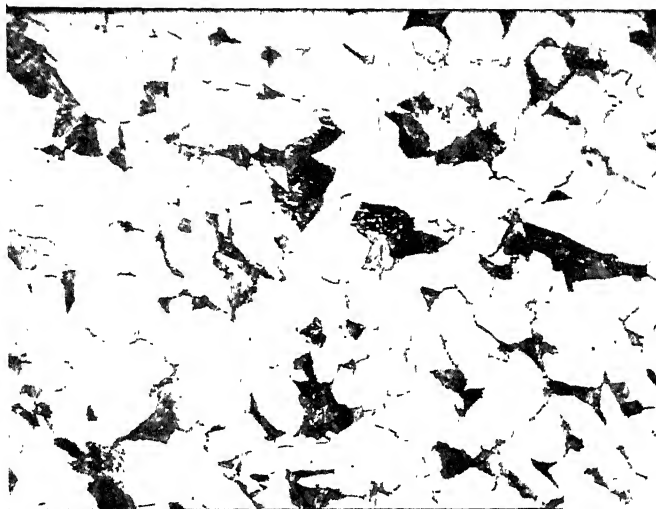
Fig. 15. Microstructure of the HSLA steel in as received condition

fibre direction might be parallel to the longitudinal axis.
The specimen has a square cross-section (10 mm x 10 mm) and
contains a 45° V notch, 2 mm deep with a 0.25 mm root radius
according to standard specifications for a charpy test, as
shown in Fig. 16.

2.1.2 Test Procedure

Charpy impact tests were carried out on a charpy
impact machine over a range of temperatures, starting from
room temperature upto $730^{\circ}C$. At the onset, a complete
cooling curve of the sample resting on the machine anvil
was obtained from a temperature starting from $800^{\circ}C$ which
gives the time taken to reach any desired test temperature
before the conduct of a series of impact tests since the tem-
perature was measured by inserting a Chromel-Alumel thermocouple
into a cylindrical hole terminating at the notch plane,
the test temperature would correspond in as far as possible
to the temperature at the plane of fracture. The cooling
curve of the sample was drawn as in Fig. (17). In an
actual test the striker of the charpy machine was released
as soon as the sample reached a test temperature and the
fracture energy noted. Tests were conducted from a low
temperature of $30^{\circ}C$ upto a temperature of $730^{\circ}C$, which
is slightly above the eutectoid temperature. Low tempera-
ture test results upto $-9^{\circ}C$ were already available from an
earlier investigation.
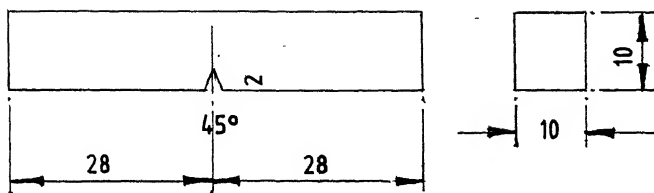
ALL DIMENSIONS IN mm

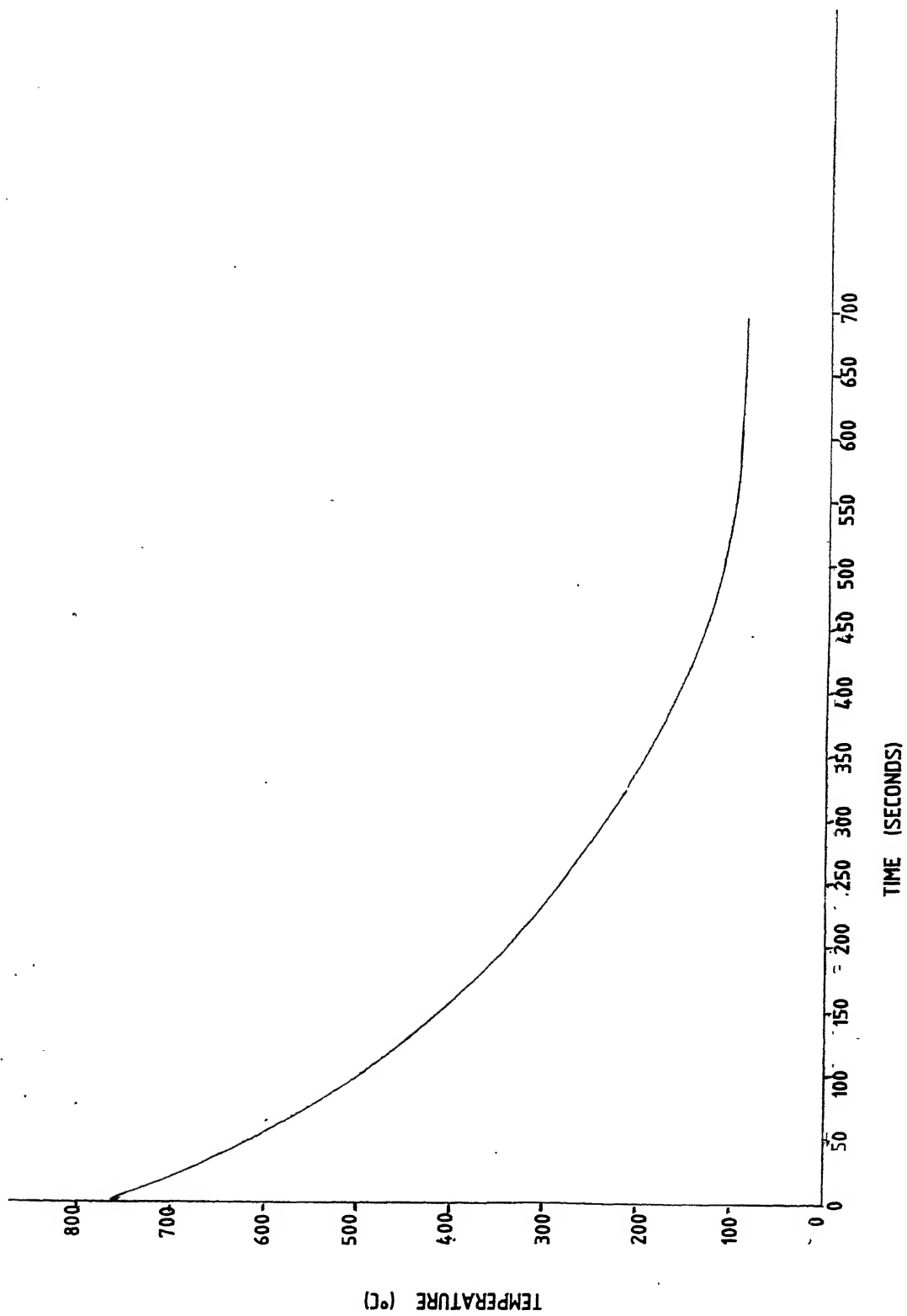Fig. 16   CHARPY TEST SAMPLE

Fig. 17   COOLING CURVE OF THE SAMPLE

2.3 OPTICAL MICROSCOPY

Samples for optical microscopy were prepared from the deformed zone of the tested samples. A cut surface taken parallel to the fracture plane was metallographically prepared and etched with Nital (3%) so as to reveal the microstructural details near the deformed zone. Most of the revealing features of the microstructure are shown in the next chapter.

2.4 ELECTRON PROBE MICRO ANALYSER AND SCANNING ELECTRON MICROSCOPY

Electron Probe Micro analysis was carried out to know the distribution of microconstituents on the fracture surface, microconstituents being Sulphur and Phosphorus. X-ray mapping of microelements has been matched with the corresponding microstructure. The instrument details are the following:

Instrument   - Electron Probe Micro Analyser

Make   - JEOL, Japan

Accelerating voltage employed - 20 KV

Probe current   - 1×10^{-8} A

Some fractographs were also separately taken in an ISI model Scanning Electron Microscope.

For EPMA and SEM samples were chosen from room temperature and 730°C so as to reveal the microstructural details at the two extremes. The salient features of the micrograph are discussed in the next chapter.

CHAPTER 3

RESULTS   AND DISCUSSIONS

3.1 IMPACT TEST RESULTS

The principal measurement from the impact charpy test is the energy required in fracturing the specimen. The energy absorbed at various temperatures ranging from sub-zero to as high as eutectoid temperature is tabulated below.

Temperature °C	Impact energy (ft-lb)	Impact energy (Joules) (1 ft lb=1.356 J)
-130	4	5.42
- 70	6	8.14
- 36	8	10.85
- 9	9	12.20
30	26	35.26
100	58	78.64
200	58	78.64
300	52	70.51
400	50	67.80
500	46	62.38
600	60	81.36
720	100	135.60
730	102	138.31

Fig.   shows plot of CVN versus temperature. In
this plot we observe that energy absorbed increase   till
100' . This increases does not occur sharply at certain
temperature. This is due to the fact that there is no one
constant temperature at which this ductile-brittle trans-
formation occurs for a given metal. The transition tempera-
ture is sensitive to a number of metallurgical variables
of which purity and grain size especially with steels
the heat treatment and even the steel making practice are
very significant variables. The effect of these variables
will be discussed later in this chapter. In this plot we
note that the impact energy decreases from 58 to 46 foot-
pound in the temperature range 100 to 600°C. This decrease
in impact energy corresponds to the plateau region in the
J versus temperature plot. This is because of dynamic strain
ageing phenomenon which occurs in this temperature range.
This phenomenon is also called 'blue brittleness' generally
observed in low carbon steels.

From CVN values, K_1 values are calculated as follows:
$$K_1 = A\,(CVN)^{1/2} \qquad \ldots \qquad (38)$$
where A is a constant having the dimension of Newton$^{-1/2}$ m^{-2}
and its numerical value depends on the test procedure and
type of steel. For the most type of steel it has been

been quoted in the literature as 15.5, but for our test procedure we calculate it from the first principle.

The relation between K_1 and J_1 is as follows:

$$J_1 = (1 - \gamma^2) \frac{K_1^2}{E} \qquad \cdots \qquad (39)$$

where is the poisson's ratio and E is the modulus of elasticity. Putting the value of K_1 from eq. (38), we have,

$$J_1 = (1 - \nu^2) \frac{[A (CVN)^{1/2}]^2}{E} \qquad \cdots \qquad (40)$$

In the above equation J_1 is a static material property whereas CVN is found out by dynamic testing involving strain rates as high as 10^5/sec. So to have a common basis, we extrapolate the JVST and CVN vs T curves to find out the value of J and CVN at $0^{\circ}K$. Since at $0^{\circ}K$ the material behaves perfectly brittle, it is reasonable to compare J and CVN. Putting in the following values, we evaluate the constant A.

$J_1 = 7.5$ KJ/m^2 at $0^{\circ}K$ from direct measurement of J from bend test.

$\gamma = 1/3$

CVN = 3 Joules at $0^{\circ}K$ from CVN test

E = 5.8 x 10^9 N/m^2 for this steel.

A comes out to be 4.04 x 10^6 Neuton$^{-1/2}$ m^{-2}. So the eq. (40) becomes ;

$$J = 2.5 \times 10^3 \, CVN$$

Using the above expression K_1 and J_1 values are calculated and tabulated below;

Temperature (°C)	CVN (Joules)	K_1 ($Nm^{-3/2}$)	J_1 (KI/m^2)
-130	5.42	9.4×10^6	13.55
- 70	8.14	11.5×10^6	20.35
- 36	10.85	13.3×10^6	27.13
- 9	12.20	14.1×10^6	30.50
30	35.26	24.0×10^6	88.15
100	78.64	35.8×10^6	196.60
200	78.64	35.8×10^6	196.60
300	70.51	33.9×10^6	176.27
400	67.80	33.3×10^6	169.50
500	62.38	31.9×10^6	155.95
600	81.36	36.4×10^6	203.40
720	135.60	47.0×10^6	339.00
730	138.31	47.5×10^6	345.80

The CVN versus temperature and J versus temperature graphs are shown in Fig. (18) and Fig. (19) respectively. Both the figures show three distinct region, namely; sharp rise upto 100°C, plateau region between 100° to 400°C and finally the rise upto 730°C. The dynamic strain aging gives rise to a plateau in the J versus temperature curve.

The occurrence of strain aging is a fairly general pheno-
menon in metals. It is due to diffusion of carbon and nitro-
gen atoms to the dislocations during the aging period to
form new atmospheres of interstitials anchoring the disloca-
tions. Support of this mechanism is found in the fact that
the activation energy for the return of the yield point
on aging in good agreement with the activation energy for the
diffusion of carbon in alpha iron.

3.1.1 Effects of Metallurgical factors on transition tempera-
ture and fracture toughness:

(a) Effect of composition:

The composition of material affects thetransition tem-
perature as well as the fracture, toughness [20] The effect
of various individual elements is discussed below.

(i) Effect of carbon and manganese:

For economic reasons, carbon is usually used as the
principal strengthening agent. Carbon is probably the most
important single factor affecting the notch toughness of
steels, raising the ductility transition temperature about
2 to 4° for each 0.01% increase in carbon content. Other
things being equal, therefore, the lower the carbon content
the lower the ductility transition temperature. Decreasing
the carbon content lowers the strength of the steel and
in order to raise it to the desired level it is generally
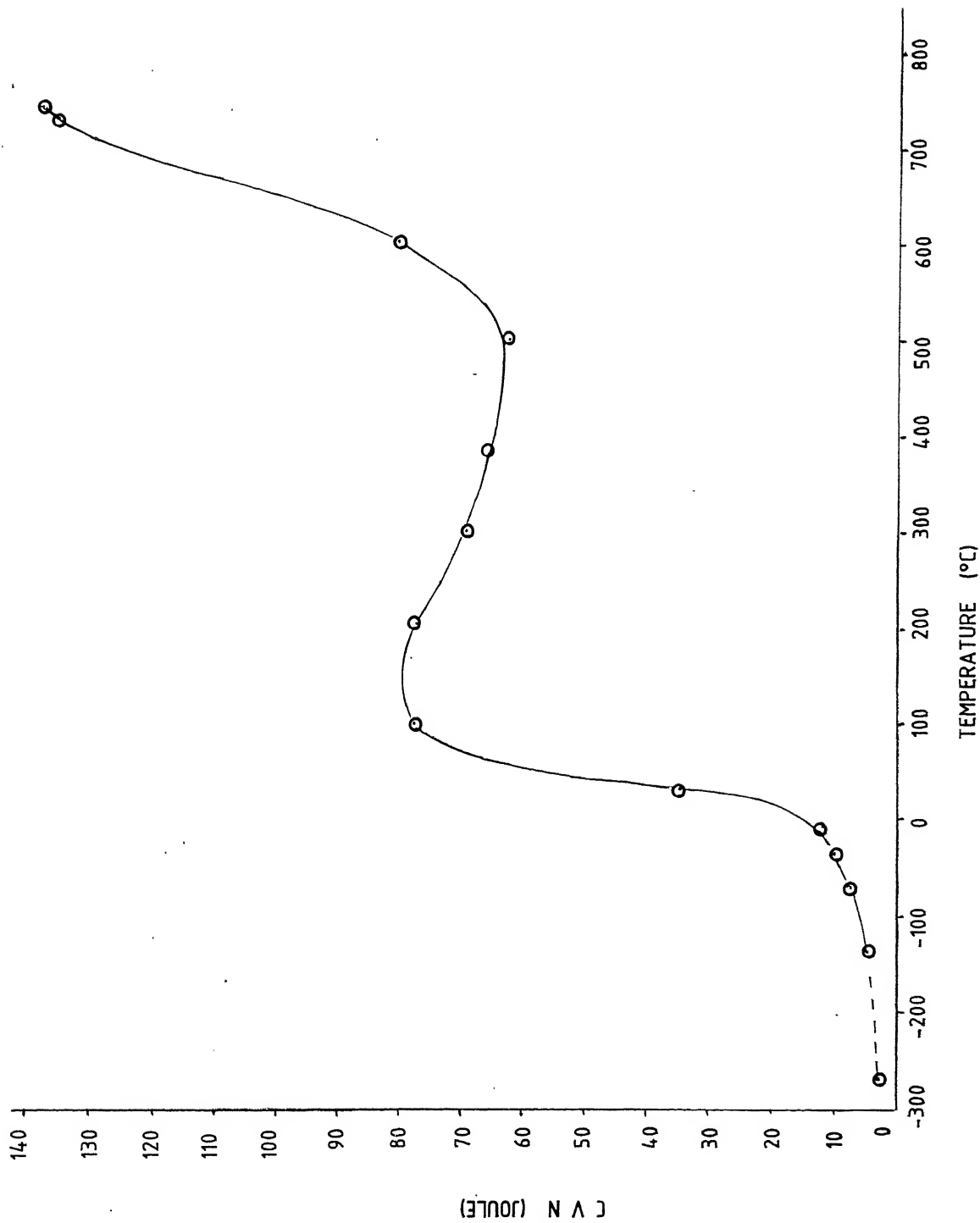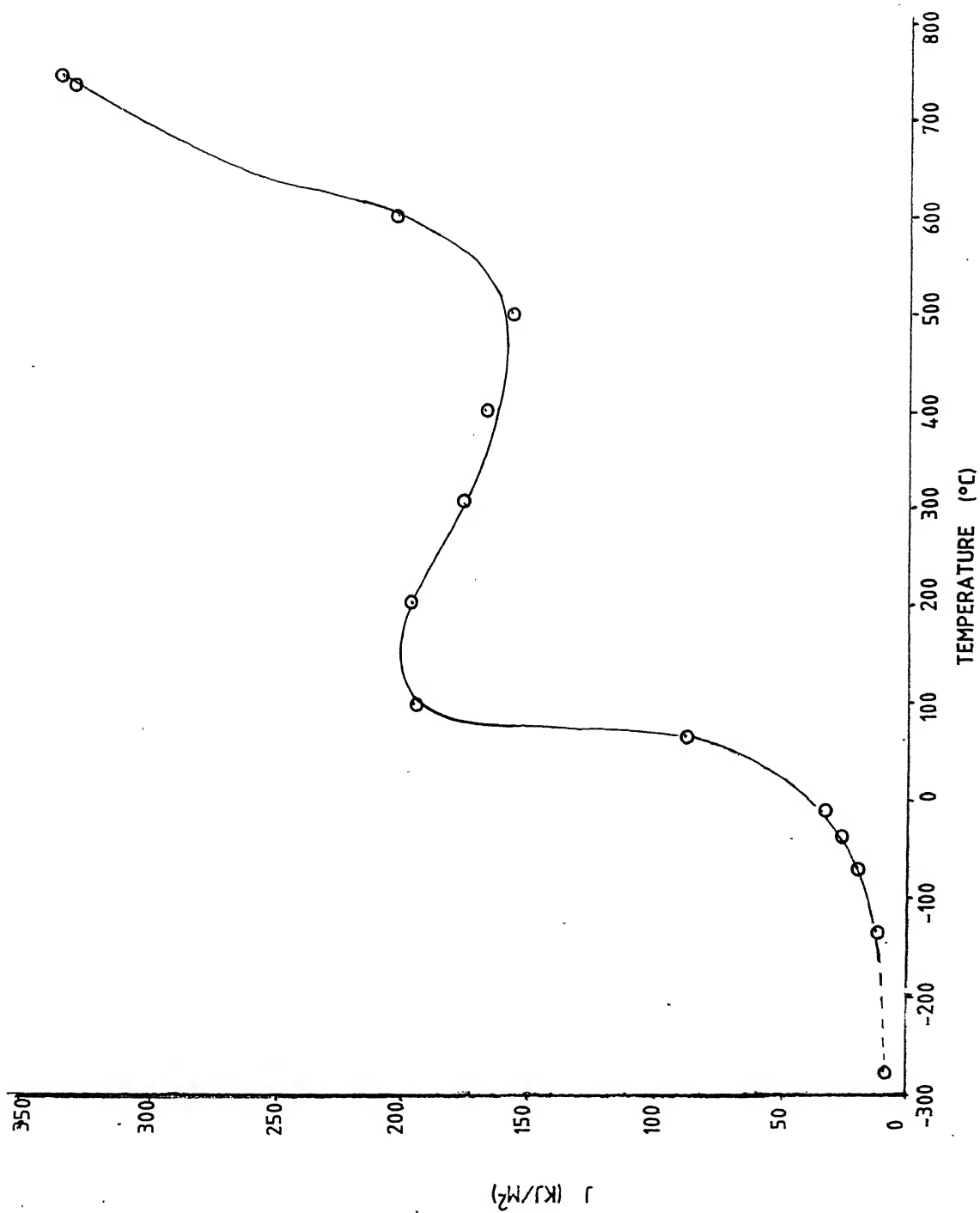necessary to add manganese.

Fig. 18 C V N vs TEMPERATURE PLOT

Fig. 19 CONVERTED J vs TEMPERATURE PLOT

Manganese is a powerful and most effective deoxidant and, apart from its influence on sulphur, is perhaps the most useful element for producing perfectly sound steel, free from internal defects such as blowholes or gas cavities. Manganese also improves the tenacity of steel without seriously affecting its ductility. Moreover, it increases the 'depth-hardness' of hardened steel. Steels law in manganese may have a shallow hardened skin even when quenched in water. When high percentages of manganese are added say between 11 and 18 percent, and the carbon content of the steel is about 1 percent, the steel is retained in the austenitic conditions when cooled in water after being heated to about $1000^{\circ}C$. Manganese by itself improves the properties of steel. Manganese has an appreciable beneficial effect on the transition temperature. Investigations have shown that each 0.01% increase in Mn content (upto about 1.5% Mn) lowers the ductility transition temperature about 1°. The fracture appearance transition temperature is also lowered but apparently to a lesser extent. Manganese in steel also prevents hot shortness and for this purpose should be present in atleast the amount of three to eight times the sulphur content.

(ii) Effect of Sulphur:

The effects of sulphur in the range of 0.02 to 0.04% on the transition temperature are not noticeable [21].

Even with high sulphur contents there seems to be little effect. However, high sulphur contents cause FeS inclusion which tend to form films, particularly at the grain boundaries. There inclusions soften at welding and hot working temperatures and may rupture. This phenomenon is known as 'hot shortners'. Therefore high sulphur contents may initiate porosity and hot cracking in welding, unless special precautions are taken. These defects can cause subsequent brittle failure by providing points from which fractures can initiate. Hot shortners may be prevented by addition of manganese to the steel since manganese has a strong affinity for sulphur, and MnS is more refractory than FeS. Since excessive addition of manganese can cause air hardening on cooling from elevated temperatures, it is usually desirable to keep sulphur contents below 0.05%.

(iii) Effect of Phosphorus:

The effect of phosphorus is even more potent than that of carbon in raising the transition temperature. Within typical commercial limits the ductility transition temperature is raised about 7 to 13° for each 0.01% of phosphorus.

(iv) Effect of other elements:

Copper does not raise the transition temperature in some low alloy steels. Cobalt, as well as nickel, tends to lower the transition temperature and has the added

virtue of not increasing hardenability.

(b) Effect of crystal structure:

The occurrence of brittle fracture is associated with the body centred cubic metals. This is more pronounced in the presence of impurities which form interstitial solid solutions. The most important element is carbon in α-iron which, even if present to the extent of only a few parts per million, will cause the metal to undergo a ductile brittle transition.

3.1.2 Composite curve:

Direct J values are taken from pre-iron work and tabulated below Figure 20 shows direct J versus temperature plot upto 340°C. Figure 21 shows direct J versus temperature and converted J versus temperature, plot.

Bend Test Results

Temperature (°C)	J_{1_2} (KJ/m²)
-170	12.82
- 59	45.01
- 21	140.07
- 10	168.92
28	190.70
101	195.20
190	186.51
260	213.00

The nature of both the curves is similar. There is scatter predominantly in the lower and higher temperature ranges. What we obtain from converting CVN values to J is the dynamic J and bend test gives the static J. The dynamic and static J values [22] are related to each other by the following expression.

$$J_{(dynamic)} = \frac{1-\alpha}{1+\alpha} \; J_{(static)}$$

where α is called relative crack speed and given by $\alpha = \frac{\dot{a}}{Co}$ where $\dot{a}$ is the crack speed and Co is the speed of sound in metals. So we can deduce that by incorporating the above correction factor both the curves would match with each other.

3.2 Optical microscopy results:

Samples are cut from the deformed zone as shown in Figure 22. Figure 23, Figure 24 and Figure 25 shows the optical micrographs in a series of temperature from room temperature to 730°C. At lower temperatures we see distinct carbide particles of Nb, V, Cr, but at higher temperatures these carbides dissolve or form cluster as precipitates.

3.2.1 Effect of microstructure on fracture toughness and transition temperature:

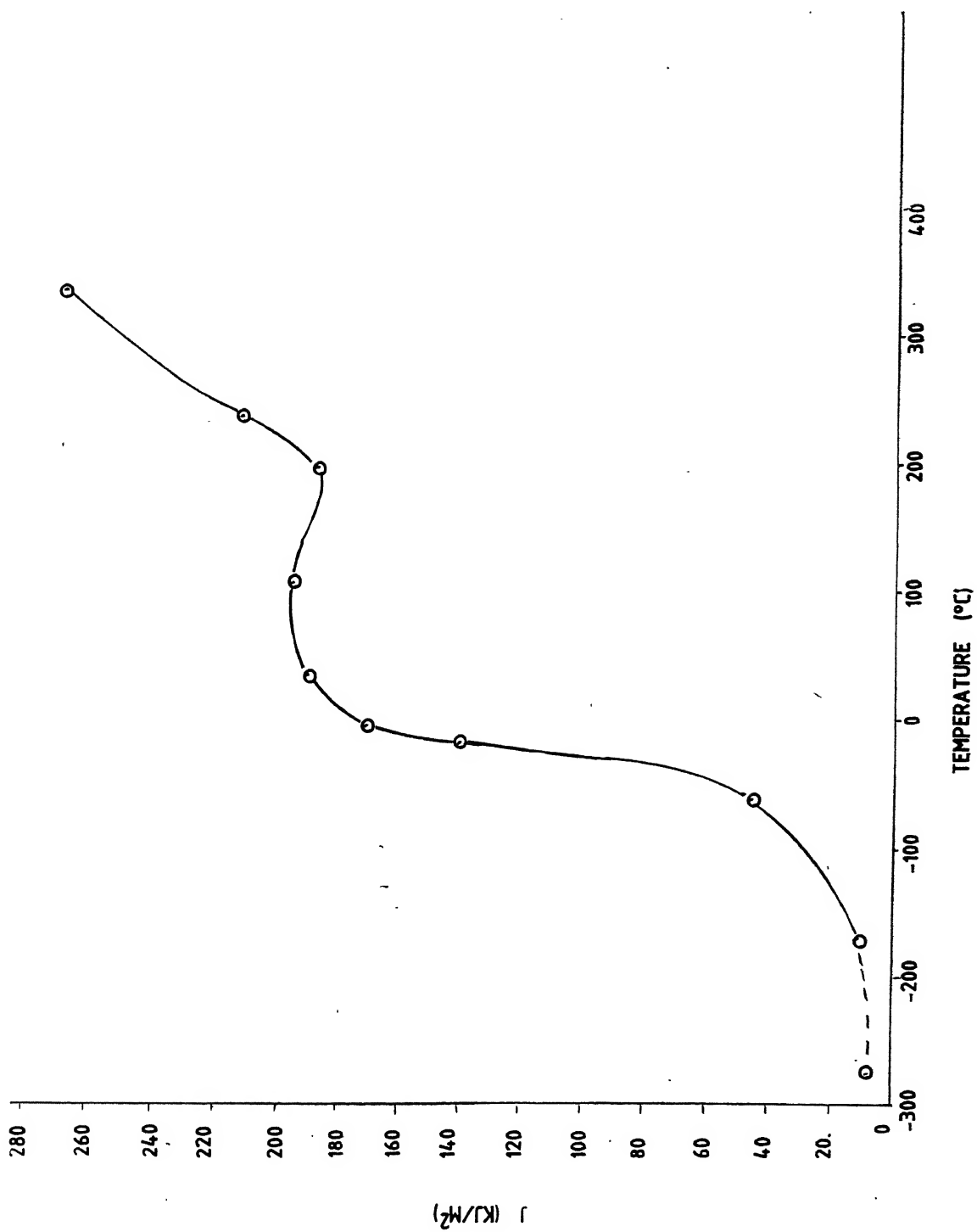At a given strength level, the transition temperature of a steel is determined by its microstructure [23]. For
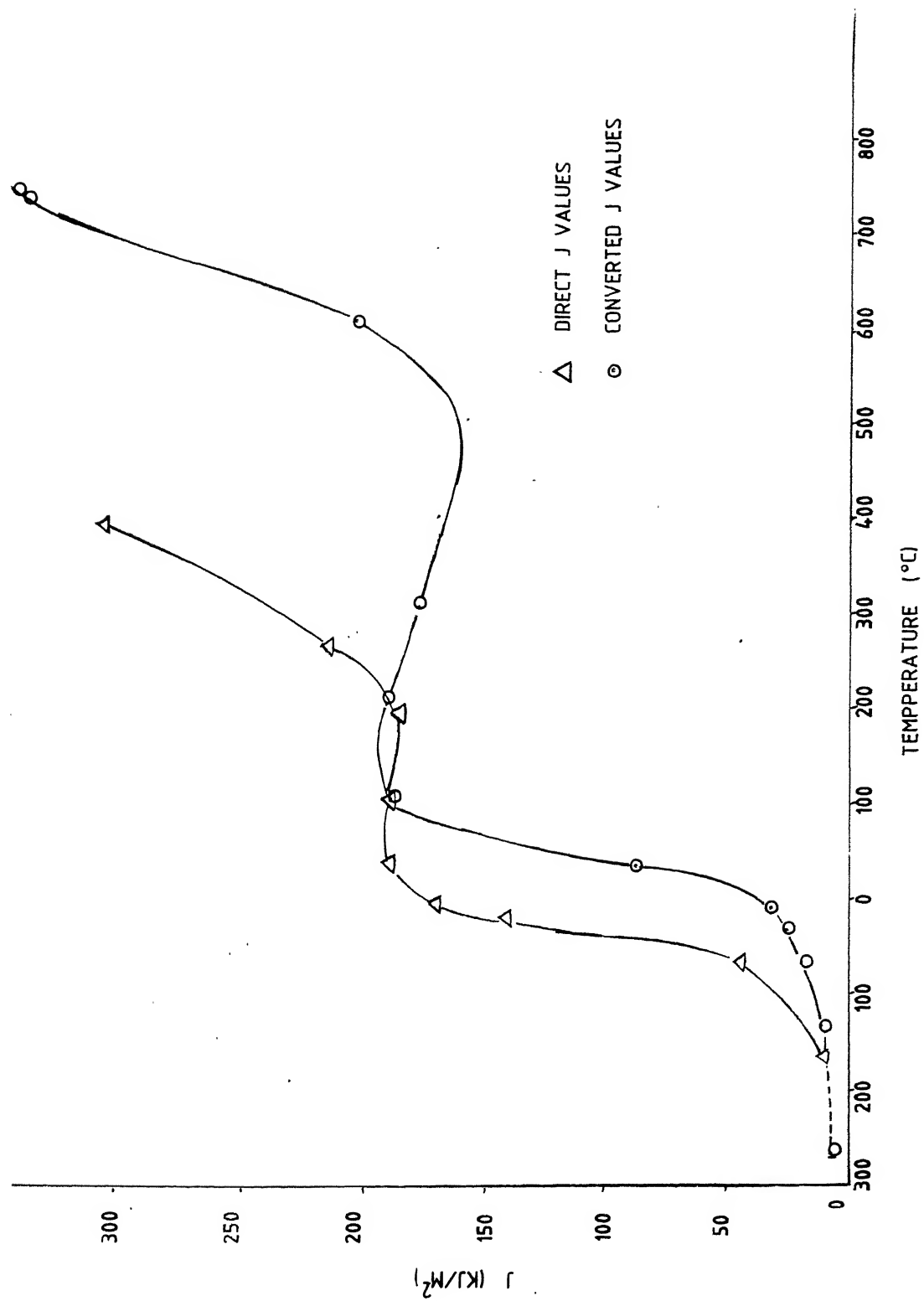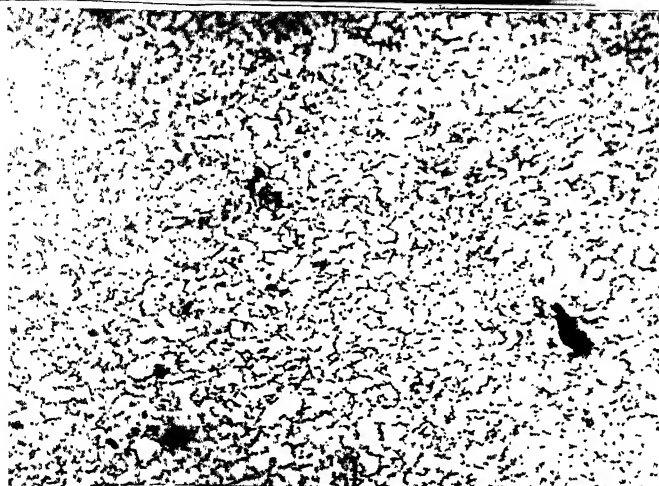
Fig. 20   DIRECT J vs TEMPERATURE PLOT

Fig. 21 COMPOSITE CURVE OF J vs TEMPERATURE

Fig. 31. Optical micrographs

    (a)   Room temperature, 200X

    (b)   100°C, 200X
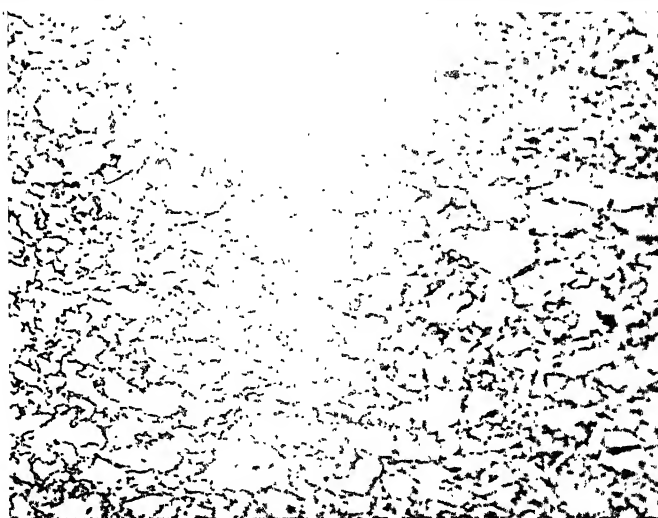
    (c)   200°C, 200X

(a)

(b)

(c)

Fig. 24.   Optical micrographs
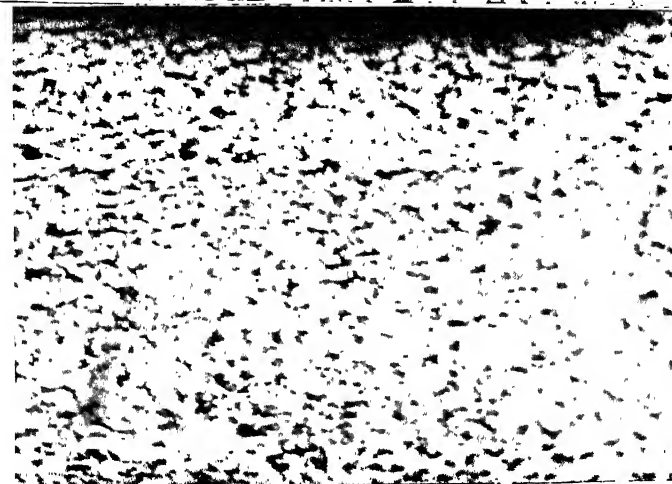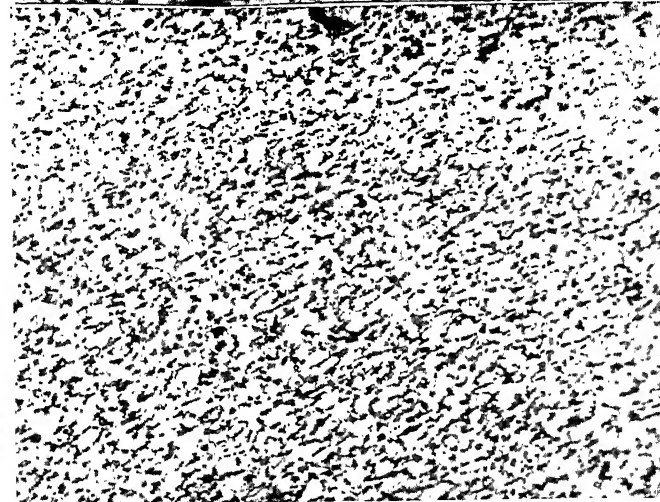
(a)   300°C, 200X

(b)   400°C, 200X

(c)   500°C, 200X

(a)

(b)

(c)

Fig. 25.   Optical micrographs
(a) 600°C, 200X
(b) 720°C, 200X
(c) 730°C, 200X

example, if the major microstructural constituents found in steels, ferrite displays the highest transition temperature, followed by pearlite, upper bainite and finally lower bainite and tempered martainite. The transition temperature of each of these constituents varies from the temperature at which the constituent formed and, where applicable, the temperature at which the steel was tempered. In practice, the cooling or quenching rate and the time-temperature transformations characteristics of a steel (including the conventional hardenability) determine the resulting microstructure or mixture of microstructures. The transformation characteristics, in turn, are controlled by the alloy composition, austenitizing temperature and austenite grainsize.

Generally, treatments that produce microstructures with inferior room temperature fracture toughness also raise transition temperature. Precipitated second phase particles are detrimental to fracture toughness, especially if located at grain boundaries. However, a spheroidization treatment can improve fracture toughness by reducing strength and eliminating ferrite plates, which are paths of easy cleavage fracture in pearlite, steels may also toughness because of various embrittlement phenomena.

Isothermally transformed lower bainite has superior fracture toughness, and a slightly lower transition temperature, then tempered martensite as the same strength. However,

mixed structures, which result from incomplete bainitic treatments causing partial transformation to martensite, have lower fracture toughness and much higher transition temperature than either 100% tempered martensite or 100% lower bainite. Thus, it is important that bainite treatments be carried to completion to avoid the adverse effects of mixed structure.

Finally, the presence of austenite inhibits the fast propagation of cleavage fracture in some ferritic and martensitic steels. From the above discussion, we can conclude the effect of microstructure on transition temperature and fracture toughness

3.3 ELECTRON PROBE MICRO ANALYSER RESULTS:

From the photographs in Figure 26 and Figure 27, we observe the distribution of micro-constituent elements phosphorus and sulphur. Sulphur exists in the form of manganese sulphide and phosphorus in the form of manganese phosphide. These two elements have deleterious effect on the mechanical properties of the material. The low value of fracture toughness can be attributed to the presence of these microconstituents. X-ray mapping shows the presence of these elements on the fracture surface and the corresponding microstructure shows the spots of MnS and MnS P_2.
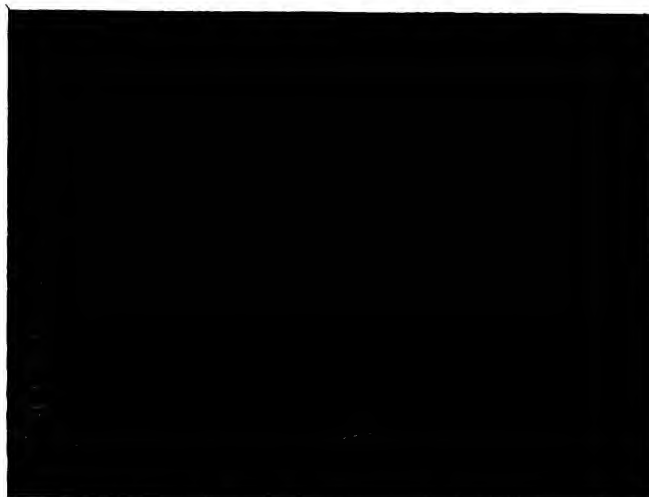
Fig. 26.   Electron probe micro analysis pictures
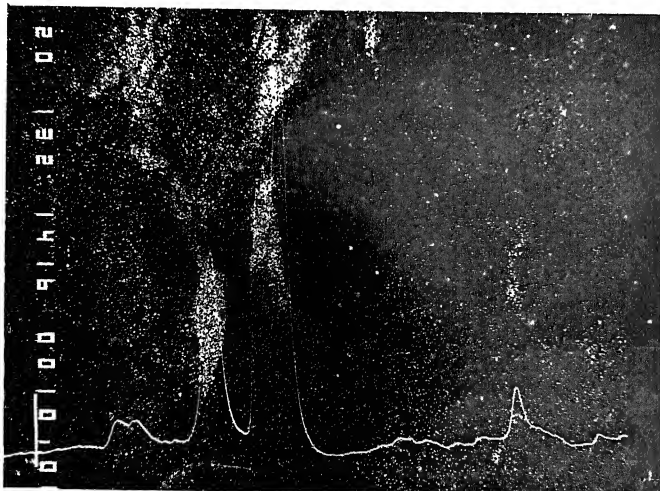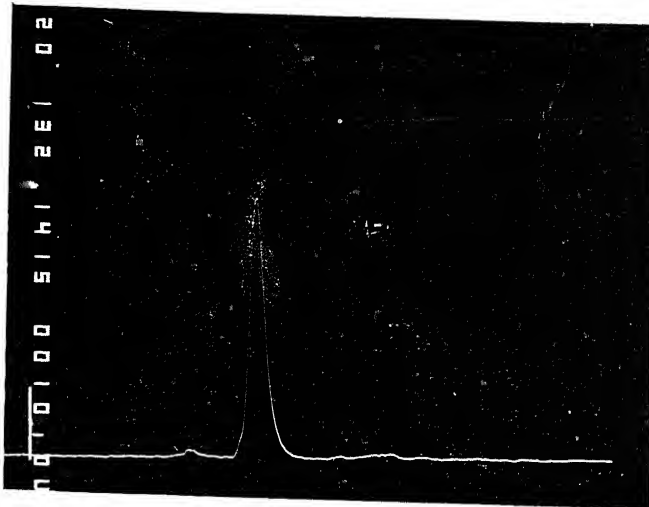showing Sulphur image at 730°C, 2000X.

Fig. 27.   Electron probe micro analysis pictures
             showing sulphur image at room temperature,
             1300X.

3.4   SCANNING ELECTRON MICROSCOPE RESULTS

Photomicrographs in Fig. (28) and Fig. (29) show
the surface features on the fracture surface at $730^{\circ}C$ and
room temperature and at two magnifications namely 200X and
15X. Surface features show that at lower temperature
the fracture is partly ductile whereas at high temperature
of $730^{\circ}C$ the fracture is completely ductile. At 15X and
200X room temperature pictures we clearly observe small
crevices which are the explanations for low fracture tough-
ness. At $730^{\circ}C$, both the pictures show the ductile type
of cleavage and show crevices. The low fracture toughness
may be attributed to the aforesaid features.

3.5   COMPARISON WITH THE LITERATURE VALUES OF J_1

Very little work has been done in this area since
the method has been only recently approved and standardized.
Consequently very little information is available. The
values obtained in our test compare well with the values
obtained by others. Our values of J_1 at room temperature
is also near to the value of Joyce [23]. He obtained the
J_{Ic} value for the type HY 130 steel which is a medium
carbon low alloy steels as ours. So the results match well
with the existing literature.
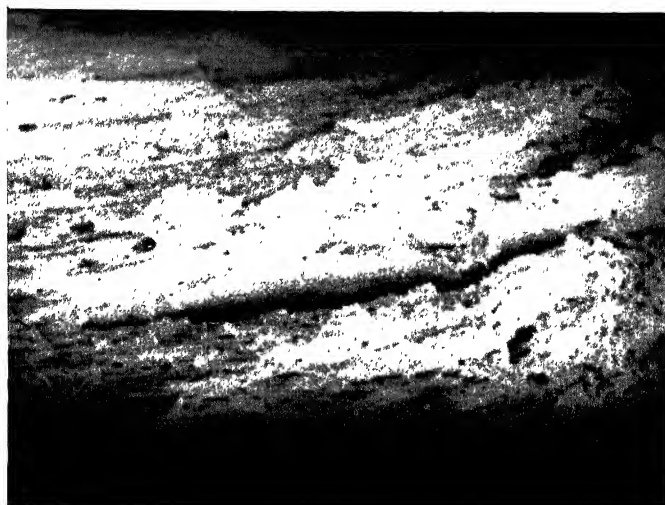
Fig. 28.   Scanning electron microscopy
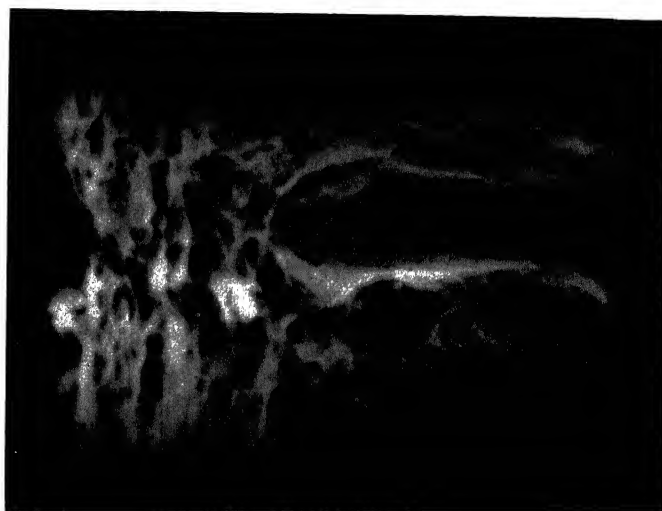   Fractographs at 730°C, 200X
              and 730°C, 15X.

Fig. 29.   Scanning electron microscopy
            Fractographs at room temperature, 200X
            and room temperature, 15X.

CONCLUSION

Converted J from CVN values versus temperature showes a plateau region between 100 and 400°C and this feature is attributed to dynamic strain aging. From the composite graph it is evident that direct J values from bend test and the converted J from CVN values match very well. The slight shift is attributed to the vast difference in the strain rates. Microstruetural features from optical, Electron probe micro analysis, Scanning electron microscopy reveal the effect of microconstituents, eg sulphur and phospherus, on fracture toughness and transition temperature. The transition temperature has been found as 35°C andthe higher value of transition temperature is because of the presence of there microconstituents. This work is a kind of first attempt to determine a detailed dependence of fracture toughness on temperature and correlate material property with microstructural.

REFERENCES

1. Griffith, A. A., 'The phenomena of rupture and flow in solids', Phil. Trans. Roy. Soc. 1921, A221, 163.

2. Orwan, E., 'Fracture and strength of solids', Rep. Prog. Phys. 1949, 12, 185.

3. Orwan, E., 'Fatigue and fracture of metals', Symp. at M. I. T., U.S.A., John Wiley & Sons, Inc., New York, 1952.

4. Irwin, G. R., and Kics, J. A., 'Fracturing and fracture dynamics', Weld. J. Res. Suppl. 1952, 17, 95S.

5. Irwin, G. R., 'Analysis of stresses and strains near the end of a crack traversing a plate', J. Appl. Mech.

   1957, 24, 361.

6. Irwin, G. R. 'Fracture on encyclopaedia of physics', Vol. VI, Springer, Heidelberg, 1958.

7. Westergaard, H. M., 'Bearing pressures and cracks', J. Appl. Mech. 1939, 61, A49.

8. Irwin, G. R., 'Analysis of stresses and strains near the end of a crack traversing a plate', Trans. ASME, J. Appl. Mech. 24, pp. 361-4.

9. Wells, A. A. (1961), 'Unstable crack propagation in metals: Cleavage and fast fracture', Symp. Crack Propagation, College of Aeronautics, Cranfield, Paper B4.

10. Cottrell, A.H., 'Theoretical aspects of radiation damage and brittle fracture in steel pressure vessels', Iron ans Steel Inst. Spec. Rep. 1961, No. 69, pp.281-96.

11. Barenblatt, G.I., 'The mathematical theory of equilibrium cracks in brittle fracture', Adv. in Appl. Mech. 1962, 7, Academic Press, New York.

12. Dugdale, D.S., 'Yielding of steel sheets containing slits', J. Mech. Phys. Solids 1960, 8, 100-104.

13. Wells, A.A., 'Unstable crack propagation in metals: cleavage and fast fracture', Crack Propagation Symposium, Cranfield, 1961.

14. Rice, J.R., 'A path independent integral and the approximate analysis of strain concentration by notches and cracks', J. Appl. Mech. 1968, 35, 379-386.

15. Hutchinson, J.W., 'Singular behaviour at the end of a tensile crack in a hardening material', J. Mechs. and Phys. of Solids 16, 1968, 13-31.

16. Rice, J.R. and Rosengren, G.F., 'Plane-strain deformation near a crack tip in a power law hardening material', J. of Mechs. and Phys. of Solids, 16, 1968, 1-12.

17. McClintock, F., 'Plasticity aspects of fracture' Fracture, Vol. III, Ed. Liebowitz, H., Academic Press, New York, 1971, pp. 47-225.

18. Broberg, K.B., 'Crack growth criteria and nonlinear fracture mechanics', J. Mechs. and Phys. of Solids, 19, 1971, pp. 407-418.

19. Rice, J.R. et al., 'Some further results of J integral analysis and estimates', in Progress in flow growth and fracture toughness testing, 1973, ASTM-STP 536, pp. 231-45.

20. Shank, M.E. et al, 'Control of Steel Construction to avoid Brittle failure'.

21. Gregory, E. and Simons, E.N., 'The Structure of Steel'.

22. Hellan Kare, 'Introduction to Fracture Mechanics'.

23. Metals Handbook, 8th Edition, Vol 10, 'Failure analysis and prevention'.

24. Joyce, J.A. and Paris, P.C., 'Direct evalution of J-resistance curves from load displacement records', Fracture Mechanics, ASTM STP 700, 1980, pp. 232-36.

25. Sih, a.c, vanElst, H.C. and Brock, D., 'Prospects of Fracture Mechanics'.